

1 We thank the reviewers for the valuable time and comments. Below, we respond to the  
2 reviewers' comments in detail and attach a marked-up manuscript (from page 8 to page  
3 44) which highlights the changes made. Referee comments are in black, italic text. Our  
4 response to referees is in black, plain text.

5

6 **Referee #1**

7 Comment 1:

8 *Current application of stable isotopes in atmospheric particulate nitrate to partition*  
9 *NO<sub>x</sub> source contributions generally presupposes that nitrogen isotopic fractionation*  
10 *during the conversion of NO<sub>x</sub> to NO<sub>3</sub><sup>-</sup> is minor. Here Chang et al. present a*  
11 *comprehensive evaluation of the nitrogen isotope fractionation during gas-to-particle*  
12 *conversion of NO<sub>x</sub> to NO<sub>3</sub><sup>-</sup>. The computational quantum chemistry is applied to*  
13 *calculate the net N isotope effect (δSN) associated with the conversion between NO<sub>x</sub>*  
14 *and NO<sub>3</sub><sup>-</sup>, and validated through a source-specific monitoring campaign. The*  
15 *applicability of this method to atmospheric aerosol samples from a megacity shows*  
16 *satisfactory results, which are in line to atmospheric chemistry modeling and to what*  
17 *one can expect in terms of source impact in a traffic-intensive environment. The source*  
18 *apportionment model to calculate nitrate fractions of different NO<sub>x</sub> sources is presented*  
19 *in a clear and concise way and is easily applicable by other researchers for similar*  
20 *studies. Great benefit with the method compared to other δ<sup>15</sup>N-based source*  
21 *apportionment studies of atmospheric nitrate is the fact that coal combustion may be*  
22 *substantively overestimated in previous studies when the N isotope fractionation during*  
23 *atmospheric nitrate formation is neglected. This makes the study with more profound*  
24 *implications. I recommend this manuscript to be published in ACP with minor revision.*

25 Reply: We appreciate the reviewer for the recognition of this work, which give us  
26 a sense of accomplishment. Below please see our point-by-point reply.

27

28 Comment 2:

29 *Title: replace “gas-particle” by “gas-to-particle”*

30 Reply: We think that it is generally appropriate to use “gas-particle” here. In the revised

31 MS, we've replaced "gas-particle" by "gas-to-particle".

32

33 Comment 3:

34 *L54: delete "nationwide,"*

35 Reply: Revised accordingly.

36

37 Comment 4:

38 *L103: add relevant reference*

39 Reply: We added Morin et al. (2008) in the revised MS.

40 Morin, S., Savarino, J., Frey, M. M., Yan, N., Bekki, S., Bottenheim, J. W., and Martins,  
41 J. M.: Tracing the origin and fate of NO<sub>x</sub> in the Arctic atmosphere using stable isotopes  
42 in nitrate, Science, 322, 730-732, doi: 10.1126/science.1161910, 2008.

43

44 Comment 5:

45 *L154-155: to my understanding, the source apportionment study of pNO<sub>3</sub>- was only*  
46 *performed in Nanjing*

47 Reply: Sorry for our mistake. We change "in order to elucidate ambient NO<sub>x</sub> sources in  
48 two distinct areas of China" to "in order to elucidate ambient NO<sub>x</sub> sources in Nanjing  
49 City of Eastern China".

50

51 Comment 6:

52 *L190: it is a bit awkward to use "heartland" here*

53 Reply: We deleted "the heartland of" in the revised MS.

54

55 Comment 7:

56 *L203-207: I didn't find the data of dicarboxylic acids and related compounds. No need*  
57 *to mention the method here*

58 Reply: We deleted the description of this method in the revised MS.

59

60 Comment 8:

61 *L317: enough credits should be given to previous researchers. L319-321: although*  
62 *described in the SI, relevant references should be added 9.*

63 Reply: Agree. Several relevant references have been added in the revised MS:

64 Parnell, A. C., Phillips, D. L., Bearhop, S., Semmens, B. X., Ward, E. J., Moore, J. W.,  
65 Jackson, A. L., Grey, J., Kelly, D. J., and Inger, R.: Bayesian stable isotope mixing  
66 models, *Environmetrics*, 24, 387-399, doi: 10.1002/env.2221, 2013.

67 Phillips, D. L., Inger, R., Bearhop, S., Jackson, A. L., Moore, J. W., Parnell, A. C.,  
68 Semmens, B. X., and Ward, E. J.: Best practices for use of stable isotope mixing  
69 models in food-web studies, *Can. J. Zool.*, 92, 823-835, doi: 10.1139/cjz-2014-0127,  
70 2014.

71 Zong, Z., Wang, X., Tian, C., Chen, Y., Fang, Y., Zhang, F., Li, C., Sun, J., Li, J., and  
72 Zhang, G.: First assessment of NO<sub>x</sub> sources at a regional background site in North  
73 China using isotopic analysis linked with modeling, *Environ. Sci. Technol.*, 51, 5923-  
74 5931, doi: 10.1021/acs.est.6b06316, 2017.

75

76 Comment 9:

77 *Figure 2b: what “MSA” stands for 10.*

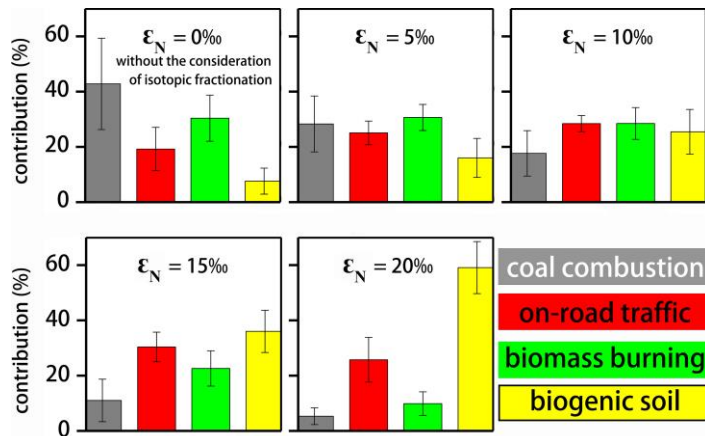
78 Reply: “MSA” stands for “methyl sulphonate”. We’ve added in the revised MS.

79

80 Comment 10

81 *Figure 6: replace “ $\hat{O}SN$ ”*

82 Reply: We guess “ $\hat{O}SN$ ” stands for “ $\epsilon N$ ”, and the reviewer want us to replace “ $\epsilon N$ ” by  
83 “ $\epsilon_N$ ”. We revised Fig. 6 as follow:



84

85

86

87 **Referee #2**

88 Comment 1:

89 *Chang et al. propose a novel method to qualitatively determine the nitrogen isotope*  
 90 *fractionation factor associated with NO<sub>x</sub> oxidation to form nitrate aerosols. The*  
 91 *authors argue that the nitrogen isotope fractionation is a fundamentally important but*  
 92 *overlooked factor in terms of influencing the source apportionment of particulate*  
 93 *nitrate, particularly in urban polluted atmosphere. The explanations given are*  
 94 *supported by strong observations, theory, and modeling. Overall, this work contributes*  
 95 *a potentially powerful new tool for the investigation of atmospheric nitrate sources, and*  
 96 *the isotopic fractionation that occurs during chemical processing. I have no major*  
 97 *concerns regarding this manuscript. As mentioned by the first reviewer, it is well written,*  
 98 *well presented and it makes sound. Beyond the remarks given by the first reviewer upon*  
 99 *which I agree, I would appreciate if the authors can also consider the following points:*

100 Reply: We are thankful for the favorable comments. Below please see our point-by-  
 101 point reply.

102

103 Comment 2:

104 *I assume that the authors have wrote a program that incorporated all of the equations*

105 *in the MS to calculate the nitrogen isotope fractionation factor and estimate nitrate*  
106 *source attribution. I believe it will be a valuable asset if the authors could make such*  
107 *program publicly available;*

108 Reply: This work was financially supported by the National Key Research and  
109 Development Program of China, which require the submission of relevant software. We  
110 have the plan to make such program publicly available. However, we prefer not to  
111 publish the software at the present stage in order to avoid compromising the future of  
112 ongoing software registration. We are willing to share the software with the reviewer  
113 for reviewing purpose.

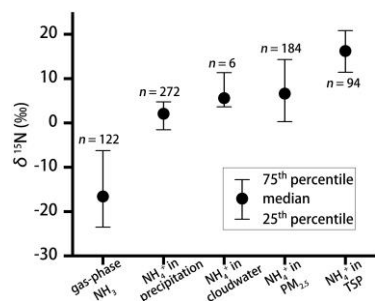
114 In “Data availability”, we will remind readers to download the software through our  
115 group website (atmosgeochem.com) after the finish of software registration.

116

117 Comment 3:

118 *compiled from previous studies, it is surprising to see no significant difference of  $\delta^{15}N$*   
119 *values among different phases of nitrate. How the authors explain my doubt;*

120 Reply: We agree with the reviewer that different phases of nitrate generally have  
121 different variation range of  $\delta^{15}N$  values. We only compiled the  $\delta^{15}N$  data of particulate  
122 nitrate and precipitation nitrate from previous publications in this study. As a  
123 compromise, below we show the variation range of  $\delta^{15}N$  values of  $NH_x$  in all phases  
124 (paper in preparation). Firstly, gaseous  $NO_x$  is as soluble as  $NH_3$  in rainwater, and the  
125 ambient concentrations of  $HONO$  and  $HNO_3$  are much lower than that of particulate  
126 nitrate. Thus, nitrate in precipitation is largely derived from particulate nitrate. In this  
127 regard, the difference of  $\delta^{15}N$  values between particulate nitrate and precipitation nitrate  
128 can be expected to lower than the difference of  $\delta^{15}N$  values between particulate  
129 ammonium and precipitation ammonium. Secondly, in this study, we have no  
130 intention to accurately the determine the location-specific values for  $\epsilon_N$  in previous  
131 studies. Instead, the  $\epsilon_N$  was assigned by a large range of  $\delta^{15}N$  values (from 0‰ to 20‰),  
132 which could significantly diminish the potential effects of the  $\delta^{15}N$  gap between  
133 particulate nitrate and precipitation nitrate on the results of nitrate source apportionment.



134

135

136 Comment 4:

137 *the use of two pathways to explain the nitrogen isotope fractionation is classic and*  
 138 *maybe correct to a large extent. I was wondering if other pathways to influence the*  
 139 *nitrogen isotope fractionation and subsequently contribute to nitrate formation need to*  
 140 *be mentioned at least;*

141 Reply: We've enriched the discussion regarding the pathways of nitrate formation in  
 142 the introduction section. Indeed, the co-editor also pointed out that the direct reactive  
 143 uptake of NO<sub>3</sub> radicals by aerosol particles also contribute to particulate nitrate. Knopf  
 144 et al. (2006, 2011) and Shiraiwa et al. (2012) have shown that NO<sub>3</sub> can be taken up  
 145 efficiently by organic (e.g., levoglucosan) aerosol and may dominate oxidation of  
 146 aerosol in the polluted urban nighttime (Kaiser et al., 2011). Globally, theoretical  
 147 modeling results show that nearly 76%, 18%, and 4% of annual inorganic nitrate are  
 148 formed via pathways/reactions involving OH, N<sub>2</sub>O<sub>5</sub>, and DMS or HC (NO<sub>3</sub> reacts with  
 149 dimethylsulfide (DMS) or hydrocarbons (HC) predominantly at night) (e.g., Alexander  
 150 et al., 2009). The stable O isotopic composition of atmospheric nitrate is a powerful  
 151 proxy for assessing which oxidation pathways are important for converting NO<sub>x</sub> into  
 152 nitrate under changing environmental conditions (e.g., polluted, volcanic events,  
 153 climate change). In the same line, in this study, the average δ<sup>18</sup>O value of pNO<sub>3</sub><sup>-</sup> in  
 154 Nanjing City was 83.0 ± 11.2‰ (see discussion later), suggesting that pNO<sub>3</sub><sup>-</sup> formation  
 155 is dominated by the pathways of "OH + NO<sub>2</sub>" and the heterogeneous hydrolysis of  
 156 N<sub>2</sub>O<sub>5</sub>.

157 Reference

158 Alexander, B., Hastings, M. G., Allman, D. J., Dachs, J., Thornton, J. A., and Kunasek,  
159 S. A.: Quantifying atmospheric nitrate formation pathways based on a global model  
160 of the oxygen isotopic composition ( $\Delta^{17}\text{O}$ ) of atmospheric nitrate, *Atmos. Chem.*  
161 *Phys.*, 9, 5043-5056, doi: 10.5194/acp-9-5043-2009, 2009.

162 Kaiser, J. C., Riemer, N., and Knopf, D. A.: Detailed heterogeneous oxidation of soot  
163 surfaces in a particle-resolved aerosol model, *Atmos. Chem. Phys.*, 11, 4505-4520,  
164 doi: 10.5194/acp-11-4505-2011, 2011.

165 Knopf, D. A., Forrester, S. M., and Slade, J. H.: Heterogeneous oxidation kinetics of  
166 organic biomass burning aerosol surrogates by  $\text{O}_3$ ,  $\text{NO}_2$ ,  $\text{N}_2\text{O}_5$ , and  $\text{NO}_3$ , *Phys. Chem.*  
167 *Chem. Phys.*, 13, 21050-21062, doi: 10.1039/C1CP22478F, 2011.

168 Knopf, D. A., Mak, J., Gross, S., and Bertram, A. K.: Does atmospheric processing of  
169 saturated hydrocarbon surfaces by  $\text{NO}_3$  lead to volatilization?, *Geophys. Res. Lett.*,  
170 33, doi:10.1029/2006GL026884, 2006.

171 Shiraiwa, M., Pöschl, U., and Knopf, D. A.: Multiphase chemical kinetics of  $\text{NO}_3$   
172 radicals reacting with organic aerosol components from biomass burning, *Environ.*  
173 *Sci. Technol.*, 46, 6630-6636, doi: 10.1021/es300677a, 2012.

174

175 Comment 5:

176 *The references in the Reference list are not always in the appropriate order: "Chang,*  
177 *Deng. . . , 2017" should come before "Chang, Liu. . . , 2016a". "Felix, J. D., and Elliott,*  
178 *E. M., 2014" should come before " Felix, J. D., Elliott, E. M., Gish, T. J. . . . , 2013".*  
179 *"Felix, J. D., Elliott, E. M., and Shaw, S. L., 2012" should come after " Felix, J. D.,*  
180 *Elliott, E. M., Gish, T. J. . . . , 2013".*

181 Reply: Revised accordingly.

182

183

184

185 Nitrogen isotope fractionation during gas-to-particle conversion of NO<sub>x</sub> to  
186 NO<sub>3</sub><sup>-</sup> in the atmosphere – implications for isotope-based NO<sub>x</sub> source  
187 apportionment

188 Yunhua Chang<sup>1</sup>, Yanlin Zhang<sup>1\*</sup>, Chongguo Tian<sup>2</sup>, Shichun Zhang<sup>3</sup>, Xiaoyan Ma<sup>4</sup>, Fang  
189 Cao<sup>1</sup>, Xiaoyan Liu<sup>1</sup>, Wenqi Zhang<sup>1</sup>, Thomas Kuhn<sup>5</sup>, and Moritz F. Lehmann<sup>5</sup>

190 <sup>1</sup>Yale-NUIST Center on Atmospheric Environment, Nanjing University of Information  
191 Science and Technology, Nanjing 10044, China

192 <sup>2</sup>Key Laboratory of Coastal Environmental Processes and Ecological Remediation,  
193 Yantai Institute of Coastal Zone Research, Chinese Academy of Sciences, Yantai  
194 264003, China

195 <sup>3</sup>Northeast Institute of Geography and Agroecology, Chinese Academy of Sciences,  
196 4888 Shengbei Road, Changchun 130102, China

197 <sup>4</sup>Key Laboratory for Aerosol Cloud-Precipitation of China Meteorological  
198 Administration, Earth System Modeling Center, Nanjing University of Information  
199 Science and Technology, Nanjing 10044, China

200 <sup>5</sup>Aquatic and Isotope Biogeochemistry, Department of Environmental Sciences,  
201 University of Basel, Basel 4056, Switzerland

202 \* Corresponding author: Yanlin Zhang

203 E-mail address: [dryanlinzhang@outlook.com](mailto:dryanlinzhang@outlook.com)

204

205

206



207 **Abstract**

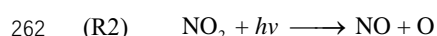
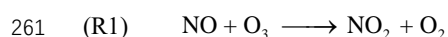
208 Atmospheric fine-particle ( $PM_{2.5}$ ) pollution is frequently associated with the formation  
209 of particulate nitrate ( $pNO_3^-$ ), the end product of the oxidation of  $NO_x$  gases ( $=NO+NO_2$ )  
210 in the upper troposphere. The application of stable nitrogen (N) (and oxygen) isotope  
211 analyses of  $pNO_3^-$  to constrain  $NO_x$  source partitioning in the atmosphere requires the  
212 knowledge of the isotope fractionation during the reactions leading to nitrate formation.  
213 Here we determined the  $\delta^{15}N$  values of fresh  $pNO_3^-$  ( $\delta^{15}N-pNO_3^-$ ) in  $PM_{2.5}$  at a rural site  
214 in Northern China, where atmospheric  $pNO_3^-$  can be attributed exclusively to biomass  
215 burning. The observed  $\delta^{15}N-pNO_3^-$  ( $12.17\pm 1.55\%$ ;  $n=8$ ) was much higher than the N  
216 isotopic source signature of  $NO_x$  from biomass burning ( $1.04\pm 4.13\%$ ). The large  
217 difference between  $\delta^{15}N-pNO_3^-$  and  $\delta^{15}N-NO_x$  ( $\Delta(\delta^{15}N)$ ) can be reconciled by the net N  
218 isotope effect ( $\epsilon_N$ ) associated with the gas-particle conversion from  $NO_x$  to  $NO_3^-$ . For  
219 the biomass-burning site, a mean  $\epsilon_N$  ( $\approx \Delta(\delta^{15}N)$ ) of  $10.99\pm 0.74\%$  was assessed through  
220 a newly-developed computational quantum chemistry (CQC) module.  $\epsilon_N$  depends on  
221 the relative importance of the two dominant N isotope exchange reactions involved  
222 ( $NO_2$  reaction with OH versus hydrolysis of dinitrogen pentoxide ( $N_2O_5$ ) with  $H_2O$ ),  
223 and varies between regions, and on a diurnal basis. A second, slightly higher CQC-  
224 based mean value for  $\epsilon_N$  ( $15.33\pm 4.90\%$ ) was estimated for an urban site with intense  
225 traffic in Eastern China, and integrated in a Bayesian isotope mixing model to make  
226 isotope-based source apportionment estimates for  $NO_x$  at this site. Based on the  $\delta^{15}N$   
227 values ( $10.93\pm 3.32\%$ ,  $n=43$ ) of ambient  $pNO_3^-$  determined for the urban site, and  
228 considering the location-specific estimate for  $\epsilon_N$ , our results reveal that the relative  
229 contribution of coal combustion and road traffic to urban  $NO_x$  are  $32\pm 1\%$  and  $68\pm 1\%$ ,  
230 respectively. This finding agrees well with a regional bottom-up emission inventory of  
231  $NO_x$ . Moreover, the variation pattern of OH contribution to ambient  $pNO_3^-$  formation  
232 calculated by the CQC module is consistent with that simulated by the Weather  
233 Research and Forecasting model coupled with Chemistry (WRF-Chem), further  
234 confirming the robustness of our estimates. Our investigations also show that, without  
235 the consideration of the N isotope effect during  $pNO_3^-$  formation, the observed  $\delta^{15}N$ -

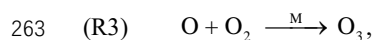
236  $p\text{NO}_3^-$  at the study site would erroneously imply that  $\text{NO}_x$  is derived almost entirely  
237 from coal combustion. Similarly, reanalysis of reported  $\delta^{15}\text{N}-\text{NO}_3^-$  data throughout  
238 China and its neighboring areas suggests that, ~~nationwide~~,  $\text{NO}_x$  emissions from coal  
239 combustion may be substantively overestimated (by >30%) when the N isotope  
240 fractionation during atmospheric  $p\text{NO}_3^-$  formation is neglected.

## 241 **1 Introduction**

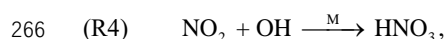
242 Nitrogen oxides ( $\text{NO}_x = \text{NO} + \text{NO}_2$ ) are among the most important molecules in  
243 tropospheric chemistry. They are involved in the formation of secondary aerosols and  
244 atmospheric oxidants, such as ozone ( $\text{O}_3$ ) and hydroxyl radicals (OH), which controls  
245 the self-cleansing capacity of the atmosphere (Galloway et al., 2003; Seinfeld and  
246 Pandis, 2012; Solomon et al., 2007). The sources of  $\text{NO}_x$  include both anthropogenic  
247 and natural origins, with more than half of the global burden ( $\sim 40 \text{ Tg N yr}^{-1}$ ) currently  
248 attributed to fossil fuel burning ( $22.4\text{-}26.1 \text{ Tg N yr}^{-1}$ ) and the rest primarily derived  
249 from nitrification/denitrification in soils (including wetlands;  $8.9 \pm 1.9 \text{ Tg N yr}^{-1}$ ),  
250 biomass burning ( $5.8 \pm 1.8 \text{ Tg N yr}^{-1}$ ), lightning ( $2\text{-}6 \text{ Tg N yr}^{-1}$ ), and oxidation of  $\text{N}_2\text{O}$   
251 in the stratosphere ( $0.1\text{-}0.6 \text{ Tg N yr}^{-1}$ ) (Jaegle et al., 2005; Richter et al., 2005; Lamsal  
252 et al., 2011; Price et al., 1997; Yienger and Levy, 1995; Miyazaki et al., 2017; Duncan  
253 et al., 2016; Anenberg et al., 2017; Levy et al., 1996). The main/ultimate sinks for  
254  $\text{NO}_x$  in the troposphere are the oxidation to nitric acid ( $\text{HNO}_{3(g)}$ ) and the formation of  
255 aerosol-phase particulate nitrate ( $p\text{NO}_3^-$ ) (Seinfeld and Pandis, 2012), the partitioning  
256 of which may vary on diurnal and seasonal time scales (Morino et al., 2006).

257 Emissions of  $\text{NO}_x$  occur mostly in the form of NO (Seinfeld and Pandis, 2012; Leighton,  
258 1961). During daytime, transformation from NO to  $\text{NO}_2$  is rapid (few minutes) and  
259 proceeds in a photochemical steady state, controlled by the oxidation of NO by  $\text{O}_3$  to  
260  $\text{NO}_2$ , and the photolysis of  $\text{NO}_2$  back to NO (Leighton, 1961):

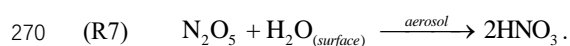
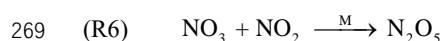
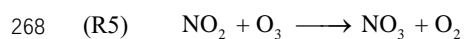




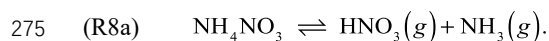
264 where M is any non-reactive species that can take up the energy released to stabilize  
265 O. NO<sub>x</sub> oxidation to HNO<sub>3</sub> is governed by the following equations. During daytime:



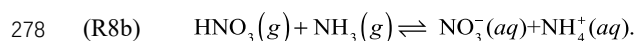
267 and during nighttime:



271 HNO<sub>3</sub> then reacts with gas-phase NH<sub>3</sub> to form ammonium nitrate (NH<sub>4</sub>NO<sub>3</sub>) aerosols.  
272 If the ambient relative humidity (RH) is lower than the efflorescence relative humidity  
273 (ERH) or crystallization relative humidity (CRH), solid-phase NH<sub>4</sub>NO<sub>3</sub>(s) is formed  
274 (Smith et al., 2012; Ling and Chan, 2007):



276 If ambient RH exceeds the ERH or CRH, HNO<sub>3</sub> and NH<sub>3</sub> dissolve into the aqueous  
277 phase (aq) (Smith et al., 2012; Ling and Chan, 2007):



279 Whilst global NO<sub>x</sub> emissions are well constrained, individual source attribution and  
280 their local or regional role in particulate nitrate formation are difficult to assess due to  
281 the short lifetime of NO<sub>x</sub> (typically less than 24 hr), and the high degree of  
282 spatiotemporal heterogeneity with regards to the ratio between gas-phase HNO<sub>3</sub> and  
283 particulate NO<sub>3</sub><sup>-</sup> (pNO<sub>3</sub><sup>-</sup>) (Duncan et al., 2016; Lu et al., 2015; Zong et al., 2017; Zhang  
284 et al., 2003). Given the conservation of the nitrogen (N) atom between NO<sub>x</sub> sources and  
285 sinks, the N isotopic composition of pNO<sub>3</sub><sup>-</sup> can be related to the different origins of the

286 emitted NO<sub>x</sub>, and thus provides valuable information on the partitioning of the NO<sub>x</sub>  
 287 sources (Morin et al., 2008). Such N isotope balance approach works best if the N  
 288 isotopic composition of various NO<sub>x</sub> sources display distinct <sup>15</sup>N/<sup>14</sup>N ratios (reported  
 289 as  $\delta^{15}\text{N} = \frac{\left(\frac{^{15}\text{N}}{^{14}\text{N}}\right)_{\text{sample}} - \left(\frac{^{15}\text{N}}{^{14}\text{N}}\right)_{\text{N}_2}}{\left(\frac{^{15}\text{N}}{^{14}\text{N}}\right)_{\text{N}_2}} \times 1000$ ). The  $\delta^{15}\text{N}$ -NO<sub>x</sub> of coal-fired power  
 290 plant (+10‰ to +25‰) (Felix et al., 2012; Heaton, 1990; Felix et al., 2013), vehicle  
 291 (+3.7‰ to +5.7‰) (Heaton, 1990; Walters et al., 2015; Felix and Elliott, 2014; Felix et  
 292 al., 2013; Wojtal et al., 2016), and biomass burning (-7‰ to +12‰) emissions (Fibiger  
 293 and Hastings, 2016), for example, are generally higher than that of lightning (-0.5‰ to  
 294 +1.4‰) (Hoering, 1957) and biogenic soil (-48.9‰ to -19.9‰) emissions (Li and Wang,  
 295 2008; Felix and Elliott, 2014; Felix et al., 2013), allowing the use of isotope mixing  
 296 models to gain insight on the NO<sub>x</sub> source apportionment for gases, aerosols, as well as  
 297 the resulting nitrate deposition (-15‰ to +15‰) (Elliott et al., 2007; Zong et al., 2017;  
 298 Savarino et al., 2007; Morin et al., 2008; Elliott et al., 2009; Park et al., 2018; Altieri et  
 299 al., 2013; Gobel et al., 2013). In addition, because of mass-independent fractionation  
 300 during its formation (Thiemens, 1999; Thiemens and Heidenreich, 1983), ozone  
 301 possesses a strong isotope anomaly ( $\Delta^{17}\text{O} \approx \delta^{17}\text{O} - 0.52 * \delta^{18}\text{O}$ ), which is propagated into  
 302 the most short-lived oxygen-bearing species, including NO<sub>x</sub> and nitrate. Therefore, the  
 303 oxygen isotopic composition of nitrate ( $\delta^{18}\text{O}$ ,  $\Delta^{17}\text{O}$ ) can provide information on the  
 304 oxidants involved in the conversion of NO<sub>x</sub> to nitrate (Michalski et al., 2003; Geng et  
 305 al., 2017). Knopf et al. (2006, 2011) and Shiraiwa et al. (2012) have shown that NO<sub>3</sub>  
 306 can be taken up efficiently by organic (e.g., levoglucosan) aerosol and may dominate  
 307 oxidation of aerosol in the polluted urban nighttime (Kaiser et al., 2011). Globally,  
 308 theoretical modeling results show that nearly 76%, 18%, and 4% of annual inorganic  
 309 nitrate are formed via pathways/reactions involving OH, N<sub>2</sub>O<sub>5</sub>, and DMS or HC (NO<sub>3</sub>  
 310 reacts with dimethylsulfide (DMS) or hydrocarbons (HC) predominantly at night) (e.g.,  
 311 Alexander et al., 2009). The stable O isotopic composition of atmospheric nitrate is a  
 312 powerful proxy for assessing which oxidation pathways are important for converting  
 313 NO<sub>x</sub> into nitrate under changing environmental conditions (e.g., polluted, volcanic  
 314 events, climate change). In the same line, in this study, the average  $\delta^{18}\text{O}$  value of  $p\text{NO}_3^-$

315 in Nanjing City was  $83.0 \pm 11.2\%$  (see discussion later), suggesting that  $p\text{NO}_3^-$   
316 formation is dominated by the pathways of “OH + NO<sub>2</sub>” and the heterogeneous  
317 hydrolysis of N<sub>2</sub>O<sub>5</sub>.

318  $\delta^{15}\text{N}$ -based source apportionment of NO<sub>x</sub> requires knowledge of how kinetic and  
319 equilibrium isotope fractionation may impact  $\delta^{15}\text{N}$  values during the conversion of NO<sub>x</sub>  
320 to nitrate (Freyer, 1978; Walters et al., 2016). If these isotope effects are considerable,  
321 they may greatly limit the use of  $\delta^{15}\text{N}$  values of  $p\text{NO}_3^-$  for NO<sub>x</sub> source partition (Walters  
322 et al., 2016). Previous studies didn't take into account the potentially biasing effect of  
323 N isotope fractionation, because they assumed that changes in the  $\delta^{15}\text{N}$  values during  
324 the conversion of NO<sub>x</sub> to nitrate are minor (without detailed explanation) (Kendall et  
325 al., 2007; Morin et al., 2008; Elliott et al., 2007) or relatively small (e.g., +3‰) (Felix  
326 and Elliott, 2014; Freyer, 2017). However, a field study by Freyer et al. (1993) has  
327 indicated that N isotope exchange may have a strong influence on the observed  $\delta^{15}\text{N}$   
328 values in atmospheric NO and NO<sub>2</sub>, implying that isotope equilibrium fractionation  
329 may play a significant role in shaping the  $\delta^{15}\text{N}$  of NO<sub>y</sub> species (the family of oxidized  
330 nitrogen molecules in the atmosphere, including NO<sub>x</sub>, NO<sub>3</sub>, NO<sub>3</sub><sup>-</sup>, peroxyacetyl nitrate  
331 etc.). The transformation of NO<sub>x</sub> to nitrate is a complex process that involves several  
332 different reaction pathways (Walters et al., 2016). To date, few fractionation factors for  
333 this conversion have been determined. Recently, Walters and Michalski (2015) and  
334 Walters et al. (2016) used computational quantum chemistry methods to calculate N  
335 isotope equilibrium fractionation factors for the exchange between major NO<sub>y</sub>  
336 molecules and confirmed theoretical predictions that <sup>15</sup>N isotopes enrich in the more  
337 oxidized form of NO<sub>y</sub>, and that the transformation of NO<sub>x</sub> to atmospheric nitrate (HNO<sub>3</sub>,  
338 NO<sub>3</sub> (aq), NO<sub>3</sub> (g)) continuously increases the  $\delta^{15}\text{N}$  in the residual NO<sub>x</sub> pool.

339 As a consequence of its severe atmospheric particle pollution during the cold season,  
340 China has made great efforts toward reducing NO<sub>x</sub> emissions from on-road traffic (e.g.,  
341 improving emission standards, higher gasoline quality, vehicle travel restrictions) (Li  
342 et al., 2017). Moreover, China has continuously implemented denitrogenation  
343 technologies (e.g., selective catalytic reduction or SCR) in the coal-fired power plants

344 sector since the mid-2000s, and has been phasing out small inefficient units (Liu et al.,  
345 2015). Monitoring and assessing the efficiency of such mitigation measures, and  
346 optimizing policy efforts to further reduce NO<sub>x</sub> emissions, requires knowledge of the  
347 vehicle- and power plant-emitted NO<sub>x</sub> to particulate nitrate in urban China (Ji et al.,  
348 2015; Fu et al., 2013; Zong et al., 2017). In this study, the chemical components of  
349 ambient fine particles (PM<sub>2.5</sub>) were quantified, and the isotopic composition of  
350 particulate nitrate ( $\delta^{15}\text{N-NO}_3^-$ ,  $\delta^{18}\text{O-NO}_3^-$ ) was assessed in order to elucidate ambient  
351 NO<sub>x</sub> sources in Nanjing City of Eastern China~~two distinct areas of China~~. We also  
352 investigated the potential isotope effect during the formation of nitrate aerosols from  
353 NO<sub>x</sub>, and evaluated how disregard of such N isotope fractionation can bias N-isotope  
354 mixing model-based estimates on the NO<sub>x</sub> source apportionment for nitrate deposition.

## 355 2 Methods

### 356 2.1 Field sampling

357 In this study, PM<sub>2.5</sub> aerosol samples were collected on precombusted (450 °C for 6 hr)  
358 quartz filters (25 × 20 cm) on a day/night basis, using high-volume air samplers at a  
359 flow rate of 1.05 m<sup>3</sup> min<sup>-1</sup> in Sanjiang and Nanjing (Fig. 1). After sampling, the filters  
360 were wrapped in aluminum foil, packed in air-tight polyethylene bags and stored at -  
361 20 °C prior to further processing and analysis. Four blank filters were also collected.  
362 They were exposed for 10 min to ambient air (i.e., without active sampling). PM<sub>2.5</sub> mass  
363 concentration was analyzed gravimetrically (Sartorius MC5 electronic microbalance)  
364 with a ± 1 µg precision before and after sampling (at 25°C and 45 ± 5% during  
365 weighing).

366

367 **Figure 1.**

368

369 The Sanjiang campaign was performed during a period of intensive burning of

370 agricultural residues between October 8 and 18, 2013, to examine if there is any  
371 significant difference between the  $\delta^{15}\text{N}$  values of  $p\text{NO}_3^-$  and  $\text{NO}_x$  emitted from biomass  
372 burning. The Sanjiang site (in the following abbreviated as SJ; 47.35°N, 133.31°E) is  
373 located at an ecological experimental station affiliated with the Chinese Academy of  
374 Sciences located in the Sanjiang Plain, a major agricultural area predominantly run by  
375 state farms in Northeastern China (Fig. 1). Surrounded by vast farm fields and bordering  
376 Far-Eastern Russia, SJ is situated in a remote and sparsely populated region, with a  
377 harsh climate and rather poorly industrialized economy. The annual mean temperature  
378 at SJ is close to the freezing point, with daily minima ranging between -31 and -15°C  
379 in the coldest month January. As a consequence of the relatively low temperatures (also  
380 during summer), biogenic production of  $\text{NO}_x$  through soil microbial processes is rather  
381 weak. SJ is therefore an excellent environment where to collect biomass burning-  
382 emitted aerosols with only minor influence from other sources.

383 The Nanjing campaign was conducted between 17 December 2014 and 8 January 2015  
384 with the main objective to examine whether N isotope measurements can be used as a  
385 tool to elucidate  $\text{NO}_x$  source contributions to ambient  $p\text{NO}_3^-$  during times of severe  
386 haze. Situated in ~~the heartland of~~ the lower Yangtze River region, Nanjing is, after  
387 Shanghai, the second largest city in Eastern China. The aerosol sampler was placed at  
388 the rooftop of a building on the Nanjing University of Information Science and  
389 Technology campus (in the following abbreviated as NJ; 18 m a.g.l.; 32.21° N, 118.72°  
390 E; Fig. 1), where  $\text{NO}_x$  emissions derive from both industrial and transportation sources.

## 391 **2.2 Laboratory analysis**

392 The mass concentrations of inorganic ions (including  $\text{SO}_4^{2-}$ ,  $\text{NO}_3^-$ ,  $\text{Cl}^-$ ,  $\text{NH}_4^+$ ,  $\text{K}^+$ ,  $\text{Ca}^{2+}$ ,  
393  $\text{Mg}^{2+}$ , and  $\text{Na}^+$ ), carbonaceous components (organic carbon or OC, elemental carbon or  
394 EC), and water-soluble organic carbon or WSOC were determined using an ion  
395 chromatograph (761 Compact IC, Metrohm, Switzerland), a thermal/optical OC/EC  
396 analyzer (RT-4 model, Sunset Lab. Inc., USA), and a TOC analyzer (Shimadzu, TOC-  
397 VCSH, Japan), respectively. Importantly, levoglucosan, a molecular marker for the

398 biomass combustion aerosols was detected using a Dionex™ ICS-5000+ system  
399 (Thermo Fisher Scientific, Sunnyvale, USA). ~~In addition, a homologous series of~~  
400 ~~dicarboxylic acids (C<sub>2</sub>-C<sub>14</sub>) and related compounds (oxoacids, α-dicarbonyls and fatty~~  
401 ~~acids) were analyzed using an Agilent 7890 gas chromatography and GC-MS detection~~  
402 ~~(Agilent Technologies, Wilmington, USA), employing a dibutyl ester derivatization~~  
403 ~~technique.~~ Chemical aerosol analyses, including sample pre-treatment, analytical  
404 procedures, protocol adaption, detection limits, and experimental uncertainty were  
405 described in detail in our previous work (Cao et al., 2016; Cao et al., 2017).

406 For isotopic analyses of aerosol nitrate, aerosol subsamples were generated by punching  
407 1.4-cm disks out of the filters. In order to extract the NO<sub>3</sub><sup>-</sup>, sample discs were placed in  
408 acid-washed glass vials with 10 ml deionized water and placed in an ultra-sonic water  
409 bath for 30 min. Between one and four disks were used for NO<sub>x</sub> extraction, dependent  
410 on the aerosol NO<sub>3</sub><sup>-</sup> content on the filters, which was determined independently. The  
411 extracts were then filtered (0.22 μm) and analyzed the next day. N and O isotope  
412 analyses of the extracted/dissolved aerosol nitrate (<sup>15</sup>N/<sup>14</sup>N, <sup>18</sup>O/<sup>16</sup>O) were performed  
413 using the denitrifier method (Sigman et al., 2001; Casciotti et al., 2002). Briefly, sample  
414 NO<sub>3</sub><sup>-</sup> is converted to nitrous oxide (N<sub>2</sub>O) by denitrifying bacteria that lack N<sub>2</sub>O  
415 reductase activity (*Pseudomonas chlororaphis* ATCC# 13985; formerly *Pseudomonas*  
416 *aureofaciens*, referred to below as such). N<sub>2</sub>O is extracted, purified, and analyzed for  
417 its N and O isotopic composition using a continuous-flow isotope ratio mass  
418 spectrometer (Thermo Finnigan Delta<sup>+</sup>, Bremen, German). Nitrate N and O isotope  
419 ratios are reported in the conventional δ-notation with respect to atmospheric N<sub>2</sub> and  
420 standard mean ocean water (V-SMOW) respectively. Analyses are calibrated using the  
421 international nitrate isotope standard IAEA-N3, with a δ<sup>15</sup>N value of 4.7‰ and a δ<sup>18</sup>O  
422 value of 25.6‰ (Böhlke et al., 2003). The blank contribution was generally lower than  
423 0.2 nmol (as compared to 20 nmol of sample N). Based on replicate measurements of  
424 standards and samples, the analytical precision for δ<sup>15</sup>N and δ<sup>18</sup>O was generally better  
425 than ± 0.2‰ and ± 0.3‰ (1σ), respectively.

426 The denitrifier method generates δ<sup>15</sup>N and δ<sup>18</sup>O values of the combined pool of NO<sub>3</sub><sup>-</sup>



427 and NO<sub>2</sub><sup>-</sup>. The presence of substantial amounts of NO<sub>2</sub><sup>-</sup> in NO<sub>3</sub><sup>-</sup> samples may lead to  
 428 errors with regards to the analysis of δ<sup>18</sup>O (Wankel et al., 2010). We refrained from  
 429 including a nitrite-removal step, because nitrite concentrations in our samples were  
 430 always < 1% of the NO<sub>3</sub><sup>-</sup> concentrations. In the following δ<sup>15</sup>N<sub>NO<sub>x</sub></sub> and δ<sup>18</sup>O<sub>NO<sub>x</sub></sub> are thus  
 431 referred to as nitrate δ<sup>15</sup>N and δ<sup>18</sup>O (or δ<sup>15</sup>N<sub>NO<sub>3</sub></sub> and δ<sup>18</sup>O<sub>NO<sub>3</sub></sub>).

432 In the case of atmospheric/aerosol nitrate samples with comparatively high δ<sup>18</sup>O values,  
 433 δ<sup>15</sup>N values tend to be overestimated by 1-2‰ (Hastings et al., 2003), if the contribution  
 434 of <sup>14</sup>N<sup>14</sup>N<sup>17</sup>O to the N<sub>2</sub>O mass 45 signal is not accounted for during isotope ratio  
 435 analysis. For most natural samples, the mass-dependent relationship can be  
 436 approximated as δ<sup>17</sup>O ≈ 0.52 × δ<sup>18</sup>O, and the δ<sup>18</sup>O can be used for the <sup>17</sup>O correction.  
 437 Atmospheric NO<sub>3</sub><sup>-</sup> does not follow this relationship but inhabits a mass-independent  
 438 component. Thus, we adopted a correction factor of 0.8 instead of 0.52 for the <sup>17</sup>O to  
 439 <sup>18</sup>O linearity (Hastings et al., 2003).

### 440 2.3 Calculation of N isotope fractionation value (ε<sub>N</sub>)

441 As we described above, the transformation process of NO<sub>x</sub> to HNO<sub>3</sub>/NO<sub>3</sub><sup>-</sup> involves  
 442 multiple reaction pathways (see also Fig. S1) and is likely to undergo isotope  
 443 equilibrium exchange reactions. The measured δ<sup>15</sup>N-NO<sub>3</sub><sup>-</sup> values of aerosol samples are  
 444 thus reflective of the combined N isotope signatures of various NO<sub>x</sub> sources (δ<sup>15</sup>N-NO<sub>x</sub>)  
 445 plus any given N isotope fractionation. Recently, Walter and Michalski (2015) used a  
 446 computational quantum chemistry approach to calculate isotope exchange fractionation  
 447 factors for atmospherically relevant NO<sub>y</sub> molecules, and based on this approach, Zong  
 448 et al. (2017) estimated the N isotope fractionation during the transformation of NO<sub>x</sub> to  
 449 pNO<sub>3</sub><sup>-</sup> at a regional background site in China. Here we adopt, and slightly modify, the  
 450 approach by Walter and Michalski (2015) and Zong et al. (2017), and assumed that the  
 451 net N isotope effect ε<sub>N</sub> (for equilibrium processes A ↔ B: ε<sub>A ↔ B</sub> =  
 452  $\left( \frac{(\text{heavy isotope/light isotope})_A}{(\text{heavy isotope/light isotope})_B} - 1 \right) \cdot 1000\text{‰}$ ; ε<sub>N</sub> refers to ε<sub>N(NO<sub>x</sub> ↔ pNO<sub>3</sub><sup>-</sup>)</sub> in this  
 453 study unless otherwise specified) during the gas-to-particle conversion from NO<sub>x</sub> to

454  $p\text{NO}_3^-$  formation ( $\Delta(\delta^{15}\text{N})_{p\text{NO}_3^-\text{NO}_x} = \delta^{15}\text{N-}p\text{NO}_3^- - \delta^{15}\text{N-NO}_x \approx \epsilon_{\text{N}}$ ) can be considered

455 a hybrid of the isotope effects of two dominant N isotopic exchange reactions:

$$456 \quad \begin{aligned} \epsilon_{\text{N}} &= \gamma \times \epsilon_{\text{N}(\text{NO}_x \leftrightarrow p\text{NO}_3^-)_{\text{OH}}} + (1-\gamma) \times \epsilon_{\text{N}(\text{NO}_x \leftrightarrow p\text{NO}_3^-)_{\text{H}_2\text{O}}} \\ &= \gamma \times \epsilon_{\text{N}(\text{NO}_x \leftrightarrow \text{HNO}_3)_{\text{OH}}} + (1-\gamma) \times \epsilon_{\text{N}(\text{NO}_x \leftrightarrow \text{HNO}_3)_{\text{H}_2\text{O}}} \end{aligned} \quad (1)$$

457 where  $\gamma$  represents the contribution from isotope fractionation by the reaction of  $\text{NO}_x$   
458 and photo-chemically produced OH to form  $\text{HNO}_3$  (and  $p\text{NO}_3^-$ ), as shown by

459  $\epsilon_{\text{N}(\text{NO}_x \leftrightarrow \text{HNO}_3)_{\text{OH}}}$  ( $\epsilon_{\text{N}(\text{NO}_x \leftrightarrow p\text{NO}_3^-)_{\text{OH}}}$ ). The remainder is formed by the hydrolysis of  $\text{N}_2\text{O}_5$

460 with aerosol water to generate  $\text{HNO}_3$  (and  $p\text{NO}_3^-$ ), namely,  $\epsilon_{\text{N}(\text{NO}_x \leftrightarrow \text{HNO}_3)_{\text{H}_2\text{O}}}$

461 ( $\epsilon_{\text{N}(\text{NO}_x \leftrightarrow p\text{NO}_3^-)_{\text{H}_2\text{O}}}$ ). Assuming that kinetic N isotope fractionation associated with the

462 reaction between  $\text{NO}_x$  and OH is negligible,  $\epsilon_{\text{N}(\text{NO}_x \leftrightarrow p\text{NO}_3^-)_{\text{OH}}}$  can be calculated based on

463 mass-balance considerations:

$$464 \quad \begin{aligned} \epsilon_{\text{N}(\text{NO}_x \leftrightarrow p\text{NO}_3^-)_{\text{OH}}} &= \epsilon_{\text{N}(\text{NO}_x \leftrightarrow \text{HNO}_3)_{\text{OH}}} = \epsilon_{\text{N}(\text{NO}_2 \leftrightarrow \text{HNO}_3)_{\text{OH}}} \\ &= 1000 \times \left[ \frac{({}^{15}\alpha_{\text{NO}_2/\text{NO}} - 1)(1 - f_{\text{NO}_2})}{(1 - f_{\text{NO}_2}) + ({}^{15}\alpha_{\text{NO}_2/\text{NO}} \times f_{\text{NO}_2})} \right] \end{aligned} \quad (2)$$

465 where  ${}^{15}\alpha_{\text{NO}_2/\text{NO}}$  is the temperature-dependent (see equation 7 and Table S1)

466 equilibrium N isotope fractionation factor between  $\text{NO}_2$  and  $\text{NO}$ , and  $f_{\text{NO}_2}$  is the

467 fraction of  $\text{NO}_2$  in the total  $\text{NO}_x$ .  $f_{\text{NO}_2}$  ranges from 0.2 to 0.95 (Walters and

468 Michalski, 2015). Similarly, assuming a negligible kinetic isotope fractionation

469 associated with the reaction  $\text{N}_2\text{O}_5 + \text{H}_2\text{O} + \text{aerosol} \rightarrow 2\text{HNO}_3$ ,  $\epsilon_{\text{N}(\text{NO}_x \leftrightarrow p\text{NO}_3^-)_{\text{H}_2\text{O}}}$  can be

470 computed from the following equation:

$$471 \quad \begin{aligned} \epsilon_{\text{N}(\text{NO}_x \leftrightarrow p\text{NO}_3^-)_{\text{H}_2\text{O}}} &= \epsilon_{\text{N}(\text{NO}_x \leftrightarrow \text{HNO}_3)_{\text{H}_2\text{O}}} = \\ &= 1000 \times ({}^{15}\alpha_{\text{N}_2\text{O}_5/\text{NO}_2} - 1) \end{aligned} \quad (3)$$

472 where  $^{15}\alpha_{\text{N}_2\text{O}_5/\text{NO}_2}$  is the equilibrium isotope fractionation factor between  $\text{N}_2\text{O}_5$  and  
 473  $\text{NO}_2$ , which also is temperature-dependent (see equation 7 and Table S1).

474 Following Walter and Michalski (2015) and Zhong et al. (2017),  $\gamma$  can then be  
 475 approximated based on the O isotope fractionation during the conversion of  $\text{NO}_x$  to  
 476  $p\text{NO}_3^-$ :

$$477 \begin{aligned} \varepsilon_{\text{O}(\text{NO}_x \leftrightarrow p\text{NO}_3^-)}_{\text{OH}} &= \gamma \times \varepsilon_{\text{O}(\text{NO}_x \leftrightarrow p\text{NO}_3^-)}_{\text{OH}} + (1 - \gamma) \times \varepsilon_{\text{O}(\text{NO}_x \leftrightarrow p\text{NO}_3^-)}_{\text{H}_2\text{O}} \\ &= \gamma \times \varepsilon_{\text{O}(\text{NO}_x \leftrightarrow \text{HNO}_3)}_{\text{OH}} + (1 - \gamma) \times \varepsilon_{\text{O}(\text{NO}_x \leftrightarrow \text{HNO}_3)}_{\text{H}_2\text{O}} \end{aligned} \quad (4)$$

478 where  $\varepsilon_{\text{O}(\text{NO}_x \leftrightarrow p\text{NO}_3^-)}_{\text{OH}}$  and  $\varepsilon_{\text{O}(\text{NO}_x \leftrightarrow p\text{NO}_3^-)}_{\text{H}_2\text{O}}$  represent the O isotope effects associated  
 479 with  $p\text{NO}_3^-$  generation through the reaction of  $\text{NO}_x$  and OH to form  $\text{HNO}_3$ , and the  
 480 hydrolysis of  $\text{N}_2\text{O}_5$  on a wetted surface to form  $\text{HNO}_3$ , respectively.  $\varepsilon_{\text{O}(\text{NO}_x \leftrightarrow p\text{NO}_3^-)}_{\text{OH}}$  can  
 481 be further expressed as:

$$482 \begin{aligned} \varepsilon_{\text{O}(\text{NO}_x \leftrightarrow p\text{NO}_3^-)}_{\text{OH}} &= \varepsilon_{\text{O}(\text{NO}_x \leftrightarrow \text{HNO}_3)}_{\text{OH}} = \frac{2}{3} \varepsilon_{\text{O}(\text{NO}_2 \leftrightarrow \text{HNO}_3)}_{\text{OH}} + \frac{1}{3} \varepsilon_{\text{O}(\text{NO} \leftrightarrow \text{HNO}_3)}_{\text{OH}} \\ &= \frac{2}{3} \left[ \frac{1000 \left( ^{18}\alpha_{\text{NO}_2/\text{NO}} - 1 \right) (1 - f_{\text{NO}_2})}{(1 - f_{\text{NO}_2}) + \left( ^{18}\alpha_{\text{NO}_2/\text{NO}} \times f_{\text{NO}_2} \right)} + \left( \delta^{18}\text{O}-\text{NO}_x \right) \right] + \\ &\quad \frac{1}{3} \left[ \left( \delta^{18}\text{O}-\text{H}_2\text{O} \right) + 1000 \left( ^{18}\alpha_{\text{OH}/\text{H}_2\text{O}} - 1 \right) \right] \end{aligned} \quad (5)$$

483 and  $\varepsilon_{\text{O}(\text{NO}_x \leftrightarrow p\text{NO}_3^-)}_{\text{H}_2\text{O}}$  can be determined as follows:

$$484 \varepsilon_{\text{O}(\text{NO}_x \leftrightarrow p\text{NO}_3^-)}_{\text{H}_2\text{O}} = \varepsilon_{\text{O}(\text{NO}_x \leftrightarrow \text{HNO}_3)}_{\text{H}_2\text{O}} = \frac{5}{6} \left( \delta^{18}\text{O}-\text{N}_2\text{O}_5 \right) + \frac{1}{6} \left( \delta^{18}\text{O}-\text{H}_2\text{O} \right) \quad (6)$$

485 where  $^{18}\alpha_{\text{NO}_2/\text{NO}}$  and  $^{18}\alpha_{\text{OH}/\text{H}_2\text{O}}$  represent the equilibrium O isotope fractionation  
 486 factors between  $\text{NO}_2$  and  $\text{NO}$ , and OH and  $\text{H}_2\text{O}$ , respectively. The range of  $\delta^{18}\text{O}-\text{H}_2\text{O}$   
 487 can be approximated using an estimated tropospheric water vapor  $\delta^{18}\text{O}$  range of -25‰-  
 488 0‰. The  $\delta^{18}\text{O}$  values for  $\text{NO}_2$  and  $\text{N}_2\text{O}_5$  range from 90‰ to 122‰ (Zong et al. 2017).

489  $^{15}\alpha_{\text{NO}_2/\text{NO}}$  and  $^{15}\alpha_{\text{N}_2\text{O}_2/\text{NO}_2}$ ,  $^{18}\alpha_{\text{NO}_2/\text{NO}}$  and  $^{18}\alpha_{\text{OH}/\text{H}_2\text{O}}$  in these equations, are dependent  
490 on the temperature, which can be expressed as:

$$491 \quad 1000(^m\alpha_{X/Y} - 1) = \frac{A}{T^4} \times 10^{10} + \frac{B}{T^3} \times 10^8 + \frac{C}{T^2} \times 10^6 + \frac{D}{T} \times 10^4 \quad (7)$$

492 where A, B, C, and D are experimental constants (Table S1) over the temperature range  
493 of 150-450 K (Walters and Michalski, 2015; Walters et al., 2016; Walters and Michalski,  
494 2016; Zong et al., 2017).

495 Based on Equations 4-7 and measured values for  $\delta^{18}\text{O}-p\text{NO}_3^-$  of ambient  $\text{PM}_{2.5}$ , a Monte  
496 Carlo simulation was performed to generate 10000 feasible solutions. The error  
497 between predicted and measured  $\delta^{18}\text{O}$  was less than 0.5%. The range (maximum and  
498 minimum) of computed contribution ratios ( $\gamma$ ) were then integrated in Equation 1 to  
499 generate an estimate range for the nitrogen isotope effect  $\epsilon_{\text{N}}$  (using Equations 2-3).  
500  $\delta^{15}\text{N}-p\text{NO}_3^-$  values can be calculated based on  $\epsilon_{\text{N}}$  and the estimated  $\delta^{15}\text{N}$  range for  
501 atmospheric  $\text{NO}_x$ , (see section 2.4).

## 502 **2.4 Bayesian isotope mixing model**

503 Isotopic mixing models allow estimating the relative contribution of multiple sources  
504 (e.g., emission sources of  $\text{NO}_x$ ) within a mixed pool (e.g., ambient  $p\text{NO}_3^-$ ). By explicitly  
505 considering the uncertainty associated with the isotopic signatures of any given source,  
506 as well as isotope fractionation during the formation of various components of a mixture,  
507 the application of Bayesian methods to stable isotope mixing models generates robust  
508 probability estimates of source proportions, and are often more appropriate when  
509 targeting natural systems than simple linear mixing models (Chang et al., 2016a). Here  
510 the Bayesian model MixSIR (a stable isotope mixing model using sampling-  
511 importance-resampling) was used to disentangle multiple  $\text{NO}_x$  sources by generating  
512 potential solutions of source apportionment as true probability distributions, which has  
513 been widely applied in a number of fields (e.g., Parnell et al., 2013; Phillips et al., 2014;  
514 Zong et al., 2017). Details on the model frame and computing methods are given in SI

515 Text S1.

516 Here, coal combustion ( $13.72 \pm 4.57\%$ ), transportation ( $-3.71 \pm 10.40\%$ ), biomass  
517 burning ( $1.04 \pm 4.13\%$ ), and biogenic emissions from soils ( $-33.77 \pm 12.16\%$ ) were  
518 considered to be the most relevant contributors of  $\text{NO}_x$  (Table S2 and Text S2). The  
519  $\delta^{15}\text{N}$  of atmospheric  $\text{NO}_x$  is unknown. However, it can be assumed that its range in the  
520 atmosphere is constrained by the  $\delta^{15}\text{N}$  of the  $\text{NO}_x$  sources and the  $\delta^{15}\text{N}$  of  $p\text{NO}_3^-$  after  
521 equilibrium fractionation conditions have been reached. Following Zong et al. (2017),  
522  $\delta^{15}\text{N}\text{-NO}_x$  in the atmosphere was determined performing iterative model simulations,  
523 with a simulation step of 0.01 times the equilibrium fractionation value based on the  
524  $\delta^{15}\text{N}\text{-NO}_x$  values of the emission sources (mean and standard deviation) and the  
525 measured  $\delta^{15}\text{N}\text{-}p\text{NO}_3^-$  of ambient  $\text{PM}_{2.5}$  (Fig. S2).

## 526 **3 Results**

### 527 **3.1 Sanjiang in Northern China**

528 The  $\delta^{15}\text{N}\text{-}p\text{NO}_3^-$  and  $\delta^{18}\text{O}\text{-}p\text{NO}_3^-$  values of the eight samples collected from the  
529 Sanjiang biomass burning field experiment, ranged from 9.54 to 13.77‰ (mean:  
530 12.17‰) and 57.17 to 75.09‰ (mean: 63.57‰), respectively. In this study, atmospheric  
531 concentrations of levoglucosan quantified from  $\text{PM}_{2.5}$  samples collected near the sites  
532 of biomass burning in Sanjiang vary between 4.0 and 20.5  $\mu\text{g m}^{-3}$ , two to five orders of  
533 magnitude higher than those measured during non-biomass burning season (Cao et al.,  
534 2017; Cao et al., 2016). Levoglucosan is an anhydrosugar formed during pyrolysis of  
535 cellulose at temperatures above 300 °C (Simoneit, 2002). Due to its specificity for  
536 cellulose combustion, it has been widely used as a molecular tracer for biomass burning  
537 (Simoneit et al., 1999; Liu et al., 2013a; Jedynska et al., 2014; Liu et al., 2014). Indeed,  
538 the concentrations of levoglucosan and aerosol nitrate in Sanjiang were highly  
539 correlated ( $R^2 = 0.64$ ; Fig. 2a), providing compelling evidence that particulate nitrate  
540 measured during our study period was predominately derived from biomass burning  
541 emissions.

### 542 3.2 Nanjing in Eastern China

543 The mass concentrations ( $mean_{min}^{max} \pm 1\sigma, n = 43$ ) of  $PM_{2.5}$  and  $pNO_3^-$  measured in Nanjing  
544 City were  $122.1_{39.0}^{227.8} \pm 47.9$  and  $17.8_{4.0}^{45.2} \pm 10.3$   $\mu g m^{-3}$ , respectively. All  $PM_{2.5}$   
545 concentrations exceeded the Chinese Air Quality Standard for daily  $PM_{2.5}$  ( $35 \mu g m^{-3}$ ),  
546 suggesting severe haze pollution during the sampling period. The corresponding  $\delta^{15}N$ -  
547  $pNO_3^-$  values (raw data without correction) ranged between 5.39‰ and 17.99‰,  
548 indicating significant enrichment in  $^{15}N$  relative to rural and coastal marine atmospheric  
549  $NO_3^-$  sources (Table S4). This may be due to the prominent contribution of fossil fuel-  
550 related  $NO_x$  emissions with higher  $\delta^{15}N$  values in urban areas (Elliott et al., 2007; Park  
551 et al., 2018).

## 552 4 Discussion

### 553 4.1 Sanjiang campaign: theoretical calculation and field validation of N isotope 554 fractionation during $pNO_3^-$ formation

555 To be used as a quantitative tracer of biomass-combustion-generated aerosols,  
556 levoglucosan must be conserved during its transport from its source, without partial  
557 removal by reactions in the atmosphere (Hennigan et al., 2010). The mass  
558 concentrations of non-sea-salt potassium ( $nss-K^+ = K^+ - 0.0355*Na^+$ ) is considered as  
559 an independent/additional indicator of biomass burning (Fig. 2b). The association of  
560 elevated levels of levoglucosan with high  $nss-K^+$  concentrations underscores that the  
561 two compounds derived from the same proximate sources, and that thus aerosol  
562 levoglucosan in Sanjiang was indeed pristine and represented a reliable source indicator  
563 that is unbiased by altering processes in the atmosphere. Moreover, in our previous  
564 work (Cao et al., 2017), we observed that there was a much greater enhancement of  
565 atmospheric  $NO_3^-$  compared to  $SO_4^{2-}$  (a typical coal-related pollutant). This additionally  
566 points to biomass burning, and not coal-combustion, as the dominant  $pNO_3^-$  source in  
567 the study area, making SJ and ideal “quasi single source” environment for calibrating

568 the N isotope effect during  $p\text{NO}_3^-$  formation.

569

570

**Figure 2.**

571

572 Our  $\delta^{18}\text{O}-p\text{NO}_3^-$  values are well within the broad range of values in previous reports  
573 (Zong et al., 2017; Geng et al., 2017; Walters and Michalski, 2016). However, as  
574 depicted in Fig. 3, the  $\delta^{15}\text{N}$  values of biomass burning-emitted  $\text{NO}_3^-$  fall within the  
575 range of  $\delta^{15}\text{N}-\text{NO}_x$  values typically reported for emissions from coal combustion,  
576 whereas they are significantly higher than the well-established values for  $\delta^{15}\text{N}-\text{NO}_x$   
577 emitted from the burning of various types of biomass (mean:  $1.04 \pm 4.13\text{‰}$ , ranging  
578 from  $-7$  to  $+12\text{‰}$ ) (Fibiger and Hastings, 2016). Turekian et al. (1998) conducted  
579 laboratory tests involving the burning of eucalyptus and African grasses, and  
580 determined that the  $\delta^{15}\text{N}$  of  $p\text{NO}_3^-$  (around  $23\text{‰}$ ) was  $6.6\text{‰}$  higher than the  $\delta^{15}\text{N}$  of the  
581 burned biomass. This implies significant N isotope partitioning during biomass burning.  
582 In the case of complete biomass combustion, by mass balance, the first gaseous  
583 products (i.e.,  $\text{NO}_x$ ) have the same  $\delta^{15}\text{N}$  as the biomass. Hence any discrepancy between  
584 the  $p\text{NO}_3^-$  and the  $\delta^{15}\text{N}$  of the biomass can be attributed to the N isotope fractionation  
585 associated with the partial conversion of gaseous  $\text{NO}_x$  to aerosol  $\text{NO}_3^-$ . Based on the  
586 computational quantum chemistry (CQC) module calculations, the N isotope  
587 fractionation  $\epsilon_N$  ( $mean_{min}^{max} \pm 1\sigma$ ) determined from the Sanjiang data was  
588  $10.99_{10.30}^{12.54} \pm 0.74\text{‰}$ . After correcting the primary  $\delta^{15}\text{N}-p\text{NO}_3^-$  values under the  
589 consideration of  $\epsilon_N$ , the resulting mean  $\delta^{15}\text{N}$  of  $1.17_{-1.89}^{2.98} \pm 1.95\text{‰}$  is very close to the  
590 N isotopic signature expected for biomass burning-emitted  $\text{NO}_x$  ( $1.04 \pm 4.13\text{‰}$ ) (Fig.  
591 3) (Fibiger and Hastings, 2016). The much higher  $\delta^{15}\text{N}-p\text{NO}_3^-$  values in our study  
592 compared to reported  $\delta^{15}\text{N}-\text{NO}_x$  values for biomass burning can easily be reconciled  
593 when including N isotope fractionation during the conversion of  $\text{NO}_x$  to  $\text{NO}_3^-$ . Put  
594 another way, given that Sanjiang is an environment where we can essentially exclude

595 NO<sub>x</sub> sources other than biomass burning at the time of sampling, the data nicely validate  
596 our CQC module-based approach to estimate  $\epsilon_N$ .

597

598 **Figure 3.**

599

#### 600 **4.2 Source apportionment of NO<sub>x</sub> in an urban setting using a Bayesian isotopic** 601 **mixing model**

602 Due to its high population density and intensive industrial production, the Nanjing  
603 atmosphere was expected to have high NO<sub>x</sub> concentrations derived from road traffic  
604 and coal combustion (Zhao et al., 2015). However, the raw  $\delta^{15}\text{N-}p\text{NO}_3^-$  values ( $10.93 \pm$   
605  $3.32\%$ ) fell well within the variation range of coal-emitted  $\delta^{15}\text{N-NO}_x$  (Fig. 3). It is  
606 tempting to conclude that coal combustion is the main, or even sole,  $p\text{NO}_3^-$  source  
607 (given the equivalent  $\delta^{15}\text{N}$  values), yet, this is very unlikely. The data rather confirm  
608 that significant isotope fractionation occurred during the conversion of NO<sub>x</sub> to NO<sub>3</sub><sup>-</sup>  
609 and that, without consideration of the N isotope effect, traffic-related NO<sub>x</sub> emissions  
610 will be markedly underestimated.

611 In the atmosphere, the oxygen atoms of NO<sub>x</sub> rapidly exchanged with O<sub>3</sub> in the NO/NO<sub>2</sub>  
612 cycle (see equations R<sub>1</sub>-R<sub>3</sub>) (Hastings et al., 2003), and the  $\delta^{18}\text{O-}p\text{NO}_3^-$  values are  
613 determined by its production pathways (R<sub>4</sub>-R<sub>7</sub>), rather than the sources of NO<sub>x</sub>  
614 (Hastings et al., 2003). Thus,  $\delta^{18}\text{O-}p\text{NO}_3^-$  can be used to gain information on the  
615 pathway of conversion of NO<sub>x</sub> to nitrate in the atmosphere (Fang et al., 2011). In the  
616 computational quantum chemistry module used here to calculate isotope fractionation,  
617 we assumed that two-thirds of the oxygen atoms in NO<sub>3</sub><sup>-</sup> derive from O<sub>3</sub> and one-third  
618 from •OH in the •OH generation pathway (R<sub>4</sub>) (Hastings et al., 2003); correspondingly,  
619 five sixths of the oxygen atoms then derived from O<sub>3</sub> and one sixth from •OH in the  
620 O<sub>3</sub>/H<sub>2</sub>O pathway (R<sub>5</sub>-R<sub>7</sub>). The assumed range for  $\delta^{18}\text{O-O}_3$  and  $\delta^{18}\text{O-H}_2\text{O}$  values were



621 90‰-122‰ and -25‰-0‰, respectively (Zong et al., 2017). The partitioning between  
622 the two possible pathways was then assessed through Monte Carlo simulation (Zong et  
623 al., 2017). The estimated range was rather broad, given the wide range of  $\delta^{18}\text{O}-\text{O}_3$  and  
624  $\delta^{18}\text{O}-\text{H}_2\text{O}$  values used. Nevertheless, the theoretical calculation of the average  
625 contribution ratio ( $\gamma$ ) for nitrate formation in Nanjing via the reaction of  $\text{NO}_2$  and  $\bullet\text{OH}$   
626 is consistent with the results from simulations using the Weather Research and  
627 Forecasting model coupled with Chemistry (WRF-Chem) (Fig. 4; see Text S3 for  
628 details). A clear diurnal cycle of the mass concentration of nitrate formed through  $\bullet\text{OH}$   
629 oxidation of  $\text{NO}_2$  can be observed (Fig. S3), with much higher concentrations between  
630 12:00 and 18:00. This indicates the importance of photochemically produced  $\bullet\text{OH}$   
631 during daytime. Yet, throughout our sampling period in Nanjing, the average  $p\text{NO}_3^-$   
632 formation by the heterogeneous hydrolysis of  $\text{N}_2\text{O}_5$  ( $12.6 \mu\text{g m}^{-3}$ ) exceeded  $p\text{NO}_3^-$   
633 formation by the reaction of  $\text{NO}_2$  and  $\bullet\text{OH}$  ( $4.8 \mu\text{g m}^{-3}$ ), even during daytime, consistent  
634 with recent observations during peak pollution periods in Beijing (Wang et al., 2017).  
635 Given that the production rates of  $\text{N}_2\text{O}_5$  in the atmosphere is governed by ambient  $\text{O}_3$   
636 concentrations, reducing atmospheric  $\text{O}_3$  levels appears to be one of the utmost  
637 important measures to take for mitigating  $p\text{NO}_3^-$  pollution in China's urban  
638 atmospheres.

639

640

#### Figure 4.

641

642 In Nanjing, dependent on the time-dependent, dominant  $p\text{NO}_3^-$  formation pathway, the  
643 average N isotope fractionation value calculated using the computational quantum  
644 chemistry module varied between 10.77‰ and 19.34‰ (15.33‰ on average). Using  
645 the Bayesian model MixSIR, the contribution of each source can be estimated, based  
646 on the mixed-source isotope data under the consideration of prior information on the  
647 site (see Text S1 for detailed information regarding model frame and computing  
648 method). As described above, theoretically, there are four major sources, i.e., road

649 traffic, coal combustion, biomass burning, and biogenic soil, potentially contributing to  
650 ambient NO<sub>x</sub>. As a start, we tentatively integrated all four sources into MixSIR (data  
651 not shown). The relative contribution of biomass burning to the ambient NO<sub>x</sub> (median  
652 value) ranged from 28% to 70% (average 42%), representing the most important source.  
653 The primary reason for such apparently high contribution by biomass burning is that  
654 the corrected  $\delta^{15}\text{N-}p\text{NO}_3^-$  values of  $-4.29_{-10.32}^{0.42} \pm 3.66\text{‰}$  are relatively close to the N  
655 isotopic signature of biomass burning-emitted NO<sub>x</sub> ( $1.04 \pm 4.13\text{‰}$ ) compared to the  
656 other possible sources. Based on  $\delta^{15}\text{N}$  alone, the isotope approach can be ambiguous if  
657 there are more than two sources. The N isotope signature of NO<sub>x</sub> from biomass burning  
658 falls right in between the spectrum of plausible values, with highest  $\delta^{15}\text{N}$  for emissions  
659 from coal combustion on the one end, and much lower values for automotive and soil  
660 emissions on the other, and will be similar to a mixed signature from coal combustion  
661 and NO<sub>x</sub> emissions from traffic.

662 We can make several evidence-based pre-assumption to better constrain the emission  
663 sources in the mixing model analysis: (1) sampling at a typical urban site in a major  
664 industrial city in China, we can assume that the sources of road traffic and coal  
665 combustion are dominant, while the contribution of biogenic soil to ambient NO<sub>x</sub>  
666 should have minimal impact, or can be largely neglected (Zhao et al., 2015); (2) there  
667 is no crop harvest activity in Eastern China during the winter season. Furthermore,  
668 deforestation and combustion of fuelwood has been discontinued in China's major  
669 cities (Chang et al., 2016a). Therefore, the contribution of biomass burning-emitted  
670 NO<sub>x</sub> during the sampling period should also be minor. Indeed, Fig. S4 shows that the  
671 mass concentration of biomass burning-related  $p\text{NO}_3^-$  is not correlated with the fraction  
672 of levoglucosan that contributes to OC, confirming a weak impact of biomass burning  
673 on the variation of  $p\text{NO}_3^-$  concentration during our study period.

674 In a second, alternative, and more realistic scenario, we excluded biomass burning and  
675 soil as potential source of NO<sub>x</sub> in MixSIR (see above). As illustrated in Fig. 5a,  
676 assuming that NO<sub>x</sub> emissions in urban Nanjing during our study period originated

677 solely from road traffic and coal combustion, their relative contribution to the mass  
678 concentration of  $p\text{NO}_3^-$  is  $12.5 \pm 9.1 \mu\text{g m}^{-3}$  (or  $68 \pm 11\%$ ) and  $4.9 \pm 2.5 \mu\text{g m}^{-3}$  (or  $32$   
679  $\pm 11\%$ ), respectively. These numbers agree well with a city-scale  $\text{NO}_x$  emission  
680 inventory established for Nanjing recently (Zhao et al., 2015). Nevertheless, on a  
681 nation-wide level, relatively large uncertainties with regards to the overall fossil fuel  
682 consumption and fuel types propagate into large uncertainties of  $\text{NO}_x$  concentration  
683 estimates and predictions of longer-term emission trends (Li et al., 2017). Current  
684 emission-inventory estimates (Jaegle et al., 2005; Zhang et al., 2012; Liu et al., 2015;  
685 Zhao et al., 2013) suggest that in 2010  $\text{NO}_x$  emissions from coal-fired power plants in  
686 China were about 30% higher than those from transportation. However, our isotope-  
687 based source apportionment of  $\text{NO}_x$  clearly shows that in 2014 the contribution from  
688 road traffic to  $\text{NO}_x$  emissions, at least in Nanjing (a city that can be considered  
689 representative for most densely populated areas in China) is twice that of coal  
690 combustion. In fact, due to changing economic activities, emission sources of air  
691 pollutants in China are changing rapidly. For example, over the past several years,  
692 China has implemented an extended portfolio of plans to phase out its old-fashioned  
693 and small power plants, and to raise the standards for reducing industrial pollutant  
694 emissions (Chang, 2012). On the other hand, China continuously experienced double-  
695 digit annual growth in terms of auto sales during the 2000s, and in 2009 it became the  
696 world's largest automobile market (Liu et al., 2013b; Chang et al., 2017; Chang et al.,  
697 2016b). Recent satellite-based studies successfully analyzed the  $\text{NO}_x$  vertical column  
698 concentration ratios for megacities in Eastern China and highlighted the importance of  
699 transportation-related  $\text{NO}_x$  emissions (Reuter et al., 2014; Gu et al., 2014; Duncan et  
700 al., 2016; Jin et al., 2017). Moreover, long-term measurements of the ratio of  $\text{NO}_3^-$   
701 versus non-sea-salt  $\text{SO}_4^{2-}$  in precipitation and aerosol jointly revealed a continuously  
702 increasing trend in Eastern China throughout the latest decade, suggesting decreasing  
703 emissions from coal combustion (Liu et al., 2013b; Itahashi et al., 2017). Both coal  
704 combustion- and road traffic-related  $p\text{NO}_3^-$  concentrations are highly correlated with  
705 their corresponding tracers (i.e.,  $\text{SO}_2$  and  $\text{CO}$ , respectively), confirming the validity of  
706 our MixSIR modelling results. With justified confidence in our Bayesian isotopic model

707 results, we conclude that previous estimates of NO<sub>x</sub> emissions from  
708 automotive/transportation sources in China based on bottom-up emission inventories  
709 may be too low.

710

711 **Figure 5.**

712

### 713 **3.3 Previous $\delta^{15}\text{N}$ -NO<sub>3</sub><sup>-</sup> based estimates on NO<sub>x</sub> sources**

714 Stable nitrogen isotope ratios of nitrate have been used to identify nitrogen sources in  
715 various environments in China, often without large differences in  $\delta^{15}\text{N}$  between  
716 rainwater and aerosol NO<sub>3</sub><sup>-</sup> (Kojima et al., 2011). In previous work, no consideration  
717 was given to potential N isotope fractionation during atmospheric pNO<sub>3</sub><sup>-</sup> formation.  
718 Here, we reevaluated 700 data points of  $\delta^{15}\text{N}$ -NO<sub>3</sub><sup>-</sup> in aerosol ( $-0.77 \pm 4.52\%$ , n = 308)  
719 and rainwater ( $3.79 \pm 6.14\%$ , n = 392) from 13 sites that are located in the area of  
720 mainland China and the Yellow and East and South China Seas (Fig. 1), extracted from  
721 the literature (see SI Table S4 for details). To verify the potentially biasing effects of  
722 neglecting N isotope fractionation (i.e. testing the sensitivity of ambient NO<sub>x</sub> source  
723 contribution estimates to the effect of N isotope fractionation), the Bayesian isotopic  
724 mixing model was applied a) to the original NO<sub>3</sub><sup>-</sup> isotope data set and b) to the corrected  
725 nitrate isotope data set, accounting for the N isotope fractionation during NO<sub>x</sub>  
726 transformation. All 13 sampling sites are located in non-urban areas; therefore, apart  
727 from coal combustion and on-road traffic, the contributions of biomass burning and  
728 biogenic soil to nitrate needs to be taken into account.

729 Although most of the sites are located in rural and coastal environments, using the  
730 original data set without the consideration of N isotope fractionation in the Bayesian  
731 isotopic mixing model, fossil fuel-related NO<sub>x</sub> emissions (coal combustion and on-road  
732 traffic) appear as the largest contributor at all the sites (data are not shown). This is

733 particularly true for coal combustion: Everywhere, except for the sites of Dongshan  
734 Islands and Mt. Lumin,  $\text{NO}_x$  emissions seem to be dominated by coal combustion. Very  
735 high contribution from coal combustion (on the order of 40-60%) particularly in  
736 Northern China may be plausible, and can be attributed to a much larger consumption  
737 of coal. Yet, rather unlikely, the highest estimated contribution of coal combustion (83%)  
738 was calculated for Beihuang Island (a full-year sampling at a costal island that is 65 km  
739 north of Shandong Peninsula and 185 km east of the Beijing-Tianjin-Hebei region) and  
740 not for mainland China. While Beihuang may be an extreme example, we argue that,  
741 collectively, the contribution of coal combustion to ambient  $\text{NO}_x$  in China as calculated  
742 on the basis of isotopic analyses in previous studies without the consideration of N  
743 isotope fractionation represent overestimates.

744 As a first step towards a more realistic assessment of the actual partitioning of  $\text{NO}_x$   
745 sources in China in general (and coal combustion-emitted  $\text{NO}_x$  in particular), it is  
746 imperative to determine the location-specific values for  $\epsilon_N$ . Unfortunately, without  
747  $\delta^{18}\text{O}\text{-NO}_3^-$  data in hand, as well as data on meteorological parameters that correspond  
748 to the 700  $\delta^{15}\text{N}\text{-NO}_3^-$  values used in our meta-analysis, it is not possible to estimate the  
749  $\epsilon_N$  values through the above-mentioned CQC module. As a viable alternative, we  
750 adopted the approximate values for  $\epsilon_N$  as estimated in Sanjiang (10.99‰) and Nanjing  
751 ( $15.33 \pm 4.90\%$ ). As indicated in Fig. 6, the estimates on the source partitioning is  
752 sensitive to the choice of  $\epsilon_N$ . Whereas with increasing  $\epsilon_N$ , estimates on the relative  
753 contribution of on-road traffic and biomass burning remained relatively stable;  
754 estimates for coal combustion and biogenic soil changed significantly, in opposite  
755 directions. More precisely, depending on  $\epsilon_N$ , the average estimate of the fractional  
756 contribution of coal combustion decreased drastically from 43% ( $\epsilon_N = 0\%$ ) to 5% ( $\epsilon_N$   
757 = 20‰) (Fig. 6), while the contribution from biogenic soil to  $\text{NO}_x$  emissions increased  
758 in a complementary way. Given the lack of better constraints on  $\epsilon_N$  for the 13 sampling  
759 sites, it cannot be our goal here to provide a robust revised estimate on the partitioning  
760 of  $\text{NO}_x$  sources throughout China and its neighboring areas. But we have very good  
761 reasons to assume that disregard of N isotope fractionation during  $p\text{NO}_3^-$  formation in

762 previous isotope-based source apportionment studies has likely led to overestimates of  
763 the relative contribution of coal combustion to total NO<sub>x</sub> emissions in China. For what  
764 we would consider the most conservative estimate, i.e. lowest calculated value for the  
765 N isotope fractionation during the transformation of NO<sub>x</sub> to pNO<sub>3</sub><sup>-</sup> ( $\epsilon_N = 5\text{‰}$ ), the  
766 approximate contribution from coal combustion to the NO<sub>x</sub> pool would be 28%, more  
767 than 30% less than N isotope mixing model-based estimates would yield without  
768 consideration of the N isotope fractionation (i.e.,  $\epsilon_N = 0\text{‰}$ ) (Fig. 6).

769

770

**Figure 6.**

771

772

#### 773 **4 Conclusion and outlook**

774 Consistent with theoretical predictions,  $\delta^{15}\text{N}$ -pNO<sub>3</sub><sup>-</sup> data from a field experiment where  
775 atmospheric pNO<sub>3</sub><sup>-</sup> formation could be attributed reliably to NO<sub>x</sub> from biomass burning  
776 only, revealed that the conversion of NO<sub>x</sub> to pNO<sub>3</sub><sup>-</sup> is associated with a significant net  
777 N isotope effect ( $\epsilon_N$ ). It is imperative that future studies, making use of isotope mixing  
778 models to gain conclusive constraints on the source partitioning of atmospheric NO<sub>x</sub>,  
779 will consider this N isotope fractionation. The latter will change with time and space,  
780 depending on the distribution of ozone and OH radicals in the atmosphere and the  
781 predominant NO<sub>x</sub> chemistry. The O-isotope signatures of pNO<sub>3</sub><sup>-</sup> is mostly chemistry-  
782 (and not source) driven (modulated by O-isotope exchange reactions in the atmosphere),  
783 and thus, O isotope measurements do not allow addressing the ambiguities with regards  
784 to the NO<sub>x</sub> source that may remain when just looking at  $\delta^{15}\text{N}$  values alone. However,  
785  $\delta^{18}\text{O}$  in pNO<sub>3</sub><sup>-</sup> will help assessing the relative importance of the dominant pNO<sub>3</sub><sup>-</sup>  
786 formation pathway. Simultaneous  $\delta^{15}\text{N}$  and  $\delta^{18}\text{O}$  measurements of atmospheric nitrate  
787 thus allow reliable information on  $\epsilon_N$ , and in turn on the relative importance of single

788 NO<sub>x</sub> sources. For example, for Nanjing, which can be considered representative for  
789 other large cities in China, dual-isotopic and chemical-tracer evidence suggest that on-  
790 road traffic and coal-fired power plants, rather than biomass burning, are the  
791 predominant sources during high-haze pollution periods. Given that the increasing  
792 frequency of nitrate-driven haze episodes in China, our findings are critically important  
793 in terms of guiding the use of stable nitrate isotope measurements to evaluate the  
794 relative importance of single NO<sub>x</sub> sources on regional scales, and for adapting suitable  
795 mitigation measures. Future assessments of NO<sub>x</sub> emissions in China (and elsewhere)  
796 should involve simultaneous  $\delta^{15}\text{N}$  and  $\delta^{18}\text{O}$  measurements of atmospheric nitrate and  
797 NO<sub>x</sub> at high spatiotemporal resolution, allowing us to more quantitatively reevaluate  
798 former N-isotope based NO<sub>x</sub> source partitioning estimates.

#### 799 **Competing interests**

800 The authors declare that they have no competing interests.

#### 801 **Data availability**

802 Data are available from the corresponding author on request. We prefer not to publish  
803 the software of calculating the nitrogen isotope fractionation factor and estimating  
804 nitrate source attribution at the present stage in order to avoid compromising the future  
805 of ongoing software registration. Readers can download the software through the  
806 website [atmosgeochem.com](http://atmosgeochem.com) after the finish of software registration.–

带格式的: 字体: (默认) Times New Roman, (中文) 等线, 小四

#### 807 ~~Acknowledgements~~ **Acknowledgement**

808 This study was supported by the National Key Research and Development Program of  
809 China (2017YFC0210101), the National Natural Science Foundation of China (Grant  
810 nos. 91644103, 41705100, and 41575129), the Provincial Natural Science Foundation  
811 of Jiangsu (BK20170946), the University Science Research Project of Jiangsu Province  
812 (17KJB170011), and through University Basel Research funds.

813

#### 814 **Reference**

带格式的: 行距: 单倍行距

- 815 [Alexander, B., Hastings, M. G., Allman, D. J., Dachs, J., Thornton, J. A., and Kunasek,](#)  
816 [S. A.: Quantifying atmospheric nitrate formation pathways based on a global model](#)  
817 [of the oxygen isotopic composition \( \$\Delta^{17}\text{O}\$ \) of atmospheric nitrate, \*Atmos. Chem.\*  
818 \[Phys., 9, 5043-5056, doi: 10.5194/acp-9-5043-2009, 2009.\]\(#\)](#)
- 819 Altieri, K. E., Hastings, M. G., Gobel, A. R., Peters, A. J., and Sigman, D. M.: Isotopic  
820 composition of rainwater nitrate at Bermuda: the influence of air mass source and  
821 chemistry in the marine boundary layer, *J. Geophys. Res.*, 118, 11, 304-311, 316,  
822 doi: 10.1002/jgrd.50829, 2013.
- 823 Anenberg, S. C., Miller, J., Minjares, R., Du, L., Henze, D. K., Lacey, F., Malley, C. S.,  
824 Emberson, L., Franco, V., Klimont, Z., and Heyes, C.: Impacts and mitigation of  
825 excess diesel-related  $\text{NO}_x$  emissions in 11 major vehicle markets, *Nature*, 545, 467-  
826 471, doi: 10.1038/nature22086, 2017.
- 827 Böhlke, J. K., Mroczkowski, S. J., and Coplen, T. B.: Oxygen isotopes in nitrate: new  
828 reference materials for  $^{18}\text{O}$ : $^{17}\text{O}$ : $^{16}\text{O}$  measurements and observations on nitrate-water  
829 equilibration, *Rapid Commun. Mass Sp.*, 17, 1835-1846, doi: 10.1002/rcm.1123,  
830 2003.
- 831 Cao, F., Zhang, S. C., Kawamura, K., and Zhang, Y. L.: Inorganic markers,  
832 carbonaceous components and stable carbon isotope from biomass burning aerosols  
833 in Northeast China, *Sci. Total Environ.*, 572, 1244-1251, doi:  
834 10.1016/j.scitotenv.2015.09.099, 2016.
- 835 Cao, F., Zhang, S. C., Kawamura, K., Liu, X., Yang, C., Xu, Z., Fan, M., Zhang, W.,  
836 Bao, M., Chang, Y., Song, W., Liu, S., Lee, X., Li, J., Zhang, G., and Zhang, Y. L.:  
837 Chemical characteristics of dicarboxylic acids and related organic compounds in  
838  $\text{PM}_{2.5}$  during biomass-burning and non-biomass-burning seasons at a rural site of  
839 Northeast China, *Environ. Pollut.*, 231, 654-662, doi: 10.1016/j.envpol.2017.08.045,  
840 2017.
- 841 Casciotti, K. L., Sigman, D. M., Hastings, M. G., Böhlke, J. K., and Hilkert, A.:  
842 Measurement of the oxygen isotopic composition of nitrate in seawater and  
843 freshwater using the denitrifier method, *Anal. Chem.*, 74, 4905-4912, doi:  
844 10.1021/ac020113w, 2002.
- 845 Chang, Y. H.: China needs a tighter  $\text{PM}_{2.5}$  limit and a change in priorities, *Environ. Sci.*  
846 *Technol.*, 46, 7069-7070, doi: 10.1021/es3022705, 2012.
- 847 [Chang, Y. H., Deng, C., Cao, F., Cao, C., Zou, Z., Liu, S., Lee, X., Li, J., Zhang, G.,](#)  
848 [and Zhang, Y.: Assessment of carbonaceous aerosols in Shanghai, China - Part I:](#)  
849 [long-term evolution, seasonal variations, and meteorological effects, \*Atmos. Chem.\*](#)  
850 [Phys., 17, 9945-9964, doi: 10.5194/acp-17-9945-2017, 2017.](#)
- 851 Chang, Y. H., Liu, X., Deng, C., Dore, A. J., and Zhuang, G.: Source apportionment of  
852 atmospheric ammonia before, during, and after the 2014 APEC summit in Beijing  
853 using stable nitrogen isotope signatures, *Atmos. Chem. Phys.*, 16, 11635-11647, doi:  
854 10.5194/acp-16-11635-2016, 2016a.
- 855 Chang, Y. H., Zou, Z., Deng, C., Huang, K., Collett, J. L., Lin, J., and Zhuang, G.: The  
856 importance of vehicle emissions as a source of atmospheric ammonia in the megacity  
857 of Shanghai, *Atmos. Chem. Phys.*, 16, 3577-3594, doi: 10.5194/acp-16-3577-2016,  
858 2016b.

带格式的: 缩进: 左侧: 0 厘米, 悬挂缩进: 1 字符, 首行缩进: -1 字符



859 [Chang, Y., Deng, C., Cao, F., Cao, C., Zou, Z., Liu, S., Lee, X., Li, J., Zhang, G., and](#)  
860 [Zhang, Y.: Assessment of carbonaceous aerosols in Shanghai, China—Part 1: long-](#)  
861 [term evolution, seasonal variations, and meteorological effects, \*Atmos. Chem. Phys.\*,](#)  
862 [17, 9945–9964, doi: 10.5194/acp-17-9945-2017, 2017.](#)

863 Duncan, B. N., Lamsal, L. N., Thompson, A. M., Yoshida, Y., Lu, Z., Streets, D. G.,  
864 Hurwitz, M. M., and Pickering, K. E.: A space-based, high-resolution view of notable  
865 changes in urban NO<sub>x</sub> pollution around the world (2005–2014), *J. Geophys. Res.*, 121,  
866 976–996, doi: 10.1002/2015JD024121, 2016.

867 Elliott, E., Kendall, C., Wankel, S. D., Burns, D., Boyer, E., Harlin, K., Bain, D., and  
868 Butler, T.: Nitrogen isotopes as indicators of NO<sub>x</sub> source contributions to atmospheric  
869 nitrate deposition across the midwestern and northeastern United States, *Environ. Sci.*  
870 *Technol.*, 41, 7661–7667, doi: 10.1021/es070898t, 2007.

871 Elliott, E. M., Kendall, C., Boyer, E. W., Burns, D. A., Lear, G. G., Golden, H. E., Harlin,  
872 K., Bytnerowicz, A., Butler, T. J., and Glatz, R.: Dual nitrate isotopes in dry  
873 deposition: Utility for partitioning NO<sub>x</sub> source contributions to landscape nitrogen  
874 deposition, *J. Geophys. Res.*, 114, doi: 10.1029/2008jg000889, 2009.

875 Fang, Y. T., Koba, K., Wang, X. M., Wen, D. Z., Li, J., Takebayashi, Y., Liu, X. Y., and  
876 Yoh, M.: Anthropogenic imprints on nitrogen and oxygen isotopic composition of  
877 precipitation nitrate in a nitrogen-polluted city in southern China, *Atmos. Chem.*  
878 *Phys.*, 11, 1313–1325, doi: 10.5194/acp-11-1313-2011, 2011.

879 ~~[Felix, J. D., Elliott, E. M., and Shaw, S. L.: Nitrogen isotopic composition of coal-fired](#)~~  
880 ~~[power plant NO<sub>x</sub>: Influence of emission controls and implications for global emission](#)~~  
881 ~~[inventories, \*Environ. Sci. Technol.\*, 46, 3528–3535, doi: 10.1021/es203355v,](#)~~  
882 ~~[2012.](#)~~~~[Felix, J. D., and Elliott, E. M.: Isotopic composition of passively collected](#)~~  
883 ~~[nitrogen dioxide emissions: Vehicle, soil and livestock source signatures, \*Atmos.\*](#)~~  
884 ~~[Environ., 92, 359–366, doi: 10.1016/j.atmosenv.2014.04.005, 2014.](#)~~

885 Felix, J. D., Elliott, E. M., Gish, T. J., McConnell, L. L., and Shaw, S. L.: Characterizing  
886 the isotopic composition of atmospheric ammonia emission sources using passive  
887 samplers and a combined oxidation-bacterial denitrifier approach, *Rapid Comm.*  
888 *Mass spec.*, 27, 2239–2246, doi: 10.1002/rcm.6679, 2013.

889 ~~[Felix, J. D., Elliott, E. M., and Shaw, S. L.: Nitrogen isotopic composition of coal-fired](#)~~  
890 ~~[power plant NO<sub>x</sub>: Influence of emission controls and implications for global emission](#)~~  
891 ~~[inventories, \*Environ. Sci. Technol.\*, 46, 3528–3535, doi: 10.1021/es203355v, 2012.](#)~~

892

893 ~~[Felix, J. D., and Elliott, E. M.: Isotopic composition of passively collected nitrogen](#)~~  
894 ~~[dioxide emissions: Vehicle, soil and livestock source signatures, \*Atmos. Environ.\*, 92,](#)~~  
895 ~~[359–366, doi: 10.1016/j.atmosenv.2014.04.005, 2014.](#)~~

896 Fibiger, D. L., and Hastings, M. G.: First measurements of the nitrogen isotopic  
897 composition of NO<sub>x</sub> from biomass burning, *Environ. Sci. Technol.*, 50, 11569–11574,  
898 doi: 10.1021/acs.est.6b03510, 2016.

899 Freyer, H. D.: Seasonal trends of NH<sub>4</sub><sup>+</sup> and NO<sub>3</sub><sup>-</sup> nitrogen isotope composition in rain  
900 collected at Jülich, Germany, *Tellus*, 30, 83–92, 1978.

901 ~~[Freyer, H. D.: Seasonal variation of <sup>15</sup>N/<sup>14</sup>N ratios in atmospheric nitrate species, \*Tellus\*,](#)~~  
902 ~~[43, 30–44, doi: 10.3402/tellusb.v43i1.15244, 2017.](#)~~

带格式的: 缩进: 左侧: 0 厘米, 悬挂缩进: 1 字符, 首行缩进: -1 字符

带格式的: 缩进: 左侧: 0 厘米, 悬挂缩进: 1 字符, 首行缩进: -1 字符

903 Freyer, H. D., Kley, D., Volz-Thomas, A., and Kobel, K.: On the interaction of isotopic  
904 exchange processes with photochemical reactions in atmospheric oxides of nitrogen,  
905 *J. Geophys. Res.*, 98, 14791-14796, doi: 10.1029/93JD00874, 1993.

906 ~~Freyer, H. D.: Seasonal variation of  $^{15}\text{N}/^{14}\text{N}$  ratios in atmospheric nitrate species, *Tellus*,  
907 *43*, 30-44, doi: 10.3402/tellusb.v43i1.15244, 2017.~~

908 Fu, X., Wang, S., Zhao, B., Xing, J., Cheng, Z., Liu, H., and Hao, J.: Emission inventory  
909 of primary pollutants and chemical speciation in 2010 for the Yangtze River Delta  
910 region, China, *Atmos. Environ.*, 70, 39-50, doi: 10.1016/j.atmosenv.2012.12.034,  
911 2013.

912 Galloway, J. N., Aber, J. D., Erisman, J. W., Seitzinger, S. P., Howarth, R. W., Cowling,  
913 E. B., and Cosby, B. J.: The nitrogen cascade, *Biosci.*, 53, 341-356, doi:  
914 10.1641/0006-3568(2003)053[0341:Tnc]2.0.Co;2, 2003.

915 Geng, L., Murray, L. T., Mickley, L. J., Lin, P., Fu, Q., Schauer, A. J., and Alexander,  
916 B.: Isotopic evidence of multiple controls on atmospheric oxidants over climate  
917 transitions, *Nature*, 546, 133-136, doi: 10.1038/nature22340, 2017.

918 Gobel, A. R., Altieri, K. E., Peters, A. J., Hastings, M. G., and Sigman, D. M.: Insights  
919 into anthropogenic nitrogen deposition to the North Atlantic investigated using the  
920 isotopic composition of aerosol and rainwater nitrate, *Geophys. Res. Lett.*, 40, 5977-  
921 5982, doi: 10.1002/2013GL058167, 2013.

922 Gu, D., Wang, Y., Smeltzer, C., and Boersma, K. F.: Anthropogenic emissions of  $\text{NO}_x$   
923 over China: Reconciling the difference of inverse modeling results using GOME-2  
924 and OMI measurements, *J. Geophys. Res.*, 119, 7732-7740, doi:  
925 10.1002/2014JD021644, 2014.

926 Hastings, M. G., Sigman, D. M., and Lipschultz, F.: Isotopic evidence for source  
927 changes of nitrate in rain at Bermuda, *J. Geophys. Res.*, 108, doi:  
928 10.1029/2003JD003789, 2003.

929 Heaton, T. H. E.:  $^{15}\text{N}/^{14}\text{N}$  ratios of  $\text{NO}_x$  from vehicle engines and coal-fired power  
930 stations, *Tellus*, 42, 304-307, doi: 10.1034/j.1600-0889.1990.00007.x-i1, 1990.

931 Hennigan, C. J., Sullivan, A. P., Collett, J. L., and Robinson, A. L.: Levoglucosan  
932 stability in biomass burning particles exposed to hydroxyl radicals, *Geophys. Res.*  
933 *Lett.*, 37, doi: 10.1029/2010GL043088, 2010.

934 Hoering, T.: The isotopic composition of the ammonia and the nitrate ion in rain,  
935 *Geochim. Cosmochim. Ac.*, 12, 97-102, doi: 10.1016/0016-7037(57)90021-2, 1957.

936 Itahashi, S., Yumimoto, K., Uno, I., Hayami, H., Fujita, S. I., Pan, Y., and Wang, Y.: A  
937 15-year record (2001-2015) of the ratio of nitrate to non-seasalt sulfate in  
938 precipitation over East Asia, *Atmos. Chem. Phys. Discuss.*, 2017, 1-30, doi:  
939 10.5194/acp-2017-848, 2017.

940 Jaegle, L., Steinberger, L., Martin, R. V., and Chance, K.: Global partitioning of  $\text{NO}_x$   
941 sources using satellite observations: Relative roles of fossil fuel combustion, biomass  
942 burning and soil emissions, *Faraday Discuss.*, 130, 407-423, doi: 10.1039/B502128F,  
943 2005.

944 Jedynska, A., Hoek, G., Wang, M., Eeftens, M., Cyrus, J., Beelen, R., Cirach, M., De  
945 Nazelle, A., Nystad, W., Makarem Akhlaghi, H., Meliefste, K., Nieuwenhuijsen, M.,  
946 de Hoogh, K., Brunekreef, B., and Kooter, I. M.: Spatial variations and development

947 of land use regression models of levoglucosan in four European study areas, *Atmos.*  
948 *Chem. Phys. Discuss.*, 2014, 13491-13527, doi: 10.5194/acpd-14-13491-2014, 2014.  
949 Ji, S., Cherry, C. R., Zhou, W., Sawhney, R., Wu, Y., Cai, S., Wang, S., and Marshall, J.  
950 D.: Environmental justice aspects of exposure to PM<sub>2.5</sub> emissions from electric  
951 vehicle use in China, *Environ. Sci. Technol.*, 49, 13912-13920, doi:  
952 10.1021/acs.est.5b04927, 2015.

953 Jin, X., Fiore, A. M., Murray, L. T., Valin, L. C., Lamsal, L. N., Duncan, B., Folkert  
954 Boersma, K., De Smedt, I., Abad, G. G., Chance, K., and Tonnesen, G. S.: Evaluating  
955 a space-based indicator of surface ozone-NO<sub>x</sub>-VOC sensitivity over midlatitude  
956 source regions and application to decadal trends, *J. Geophys. Res.*, 122, 439-461, doi:  
957 10.1002/2017JD026720, 2017.

958 Kaiser, J. C., Riemer, N., and Knopf, D. A.: Detailed heterogeneous oxidation of soot  
959 surfaces in a particle-resolved aerosol model, *Atmos. Chem. Phys.*, 11, 4505-4520,  
960 doi: 10.5194/acp-11-4505-2011, 2011.

961

962 Kendall, C., Elliott, E. M., and Wankel, S. D.: Stable isotopes in ecology and  
963 environmental science, chapter 12, 2<sup>nd</sup> Edition, Blackwell, Oxford, 2007.

964 Knopf, D. A., Forrester, S. M., and Slade, J. H.: Heterogeneous oxidation kinetics of  
965 organic biomass burning aerosol surrogates by O<sub>3</sub>, NO<sub>2</sub>, N<sub>2</sub>O<sub>5</sub>, and NO<sub>3</sub>, *Phys. Chem.*  
966 *Chem. Phys.*, 13, 21050-21062, doi: 10.1039/C1CP22478F, 2011.

967 Knopf, D. A., Mak, J., Gross, S., and Bertram, A. K.: Does atmospheric processing of  
968 saturated hydrocarbon surfaces by NO<sub>3</sub> lead to volatilization?, *Geophys. Res. Lett.*,  
969 33, doi:10.1029/2006GL026884, 2006.

970 Kojima, K., Murakami, M., Yoshimizu, C., Tayasu, I., Nagata, T., and Furumai, H.:  
971 Evaluation of surface runoff and road dust as sources of nitrogen using nitrate  
972 isotopic composition, *Chemosphere*, 84, 1716-1722, doi:  
973 10.1016/j.chemosphere.2011.04.071, 2011.

974 Lamsal, L. N., Martin, R. V., Padmanabhan, A., van Donkelaar, A., Zhang, Q., Sioris,  
975 C. E., Chance, K., Kurosu, T. P., and Newchurch, M. J.: Application of satellite  
976 observations for timely updates to global anthropogenic NO<sub>x</sub> emission inventories,  
977 *Geophys. Res. Lett.*, 38, doi: 10.1029/2010GL046476, 2011.

978 Leighton, P.: *Photochemistry of Air Pollution*, Academic, New York, 1961.

979 Levy, H., Moxim, W. J., and Kasibhatla, P. S.: A global three-dimensional time-  
980 dependent lightning source of tropospheric NO<sub>x</sub>, *J. Geophys. Res.*, 101, 22911-22922,  
981 doi: 10.1029/96JD02341, 1996.

982 Li, D., and Wang, X.: Nitrogen isotopic signature of soil-released nitric oxide (NO)  
983 after fertilizer application, *Atmos. Environ.*, 42, 4747-4754, doi:  
984 10.1016/j.atmosenv.2008.01.042, 2008.

985 Li, M., Zhang, Q., Kurokawa, J. I., Woo, J. H., He, K., Lu, Z., Ohara, T., Song, Y.,  
986 Streets, D. G., Carmichael, G. R., Cheng, Y., Hong, C., Huo, H., Jiang, X., Kang, S.,  
987 Liu, F., Su, H., and Zheng, B.: MIX: a mosaic Asian anthropogenic emission  
988 inventory under the international collaboration framework of the MICS-Asia and  
989 HTAP, *Atmos. Chem. Phys.*, 17, 935-963, doi: 10.5194/acp-17-935-2017, 2017.

990 Ling, T. Y., and Chan, C. K.: Formation and transformation of metastable double salts

带格式的: 行距: 单倍行距

带格式的: 正文, 左

带格式的: 行距: 单倍行距

带格式的: 正文, 左, 缩进: 左侧: 0 厘米, 悬挂缩进: 1 字符,  
首行缩进: -1 字符

991 from the crystallization of mixed ammonium nitrate and ammonium sulfate particles,  
992 Environ. Sci. Technol., 41, 8077-8083, doi: 10.1021/es071419t, 2007.

993 Liu, D., Li, J., Zhang, Y., Xu, Y., Liu, X., Ding, P., Shen, C., Chen, Y., Tian, C., and  
994 Zhang, G.: The use of levoglucosan and radiocarbon for source apportionment of  
995 PM<sub>2.5</sub> carbonaceous aerosols at a background site in East China, Environ. Sci.  
996 Technol., 47, 10454-10461, doi: 10.1021/es401250k, 2013a.

997 Liu, F., Zhang, Q., Tong, D., Zheng, B., Li, M., Huo, H., and He, K. B.: High-resolution  
998 inventory of technologies, activities, and emissions of coal-fired power plants in  
999 China from 1990 to 2010, Atmos. Chem. Phys., 15, 13299-13317, doi: 10.5194/acp-  
1000 15-13299-2015, 2015.

1001 Liu, J., Li, J., Zhang, Y., Liu, D., Ding, P., Shen, C., Shen, K., He, Q., Ding, X., Wang,  
1002 X., Chen, D., Szidat, S., and Zhang, G.: Source apportionment using radiocarbon and  
1003 organic tracers for PM<sub>2.5</sub> carbonaceous aerosols in Guangzhou, South China:  
1004 contrasting local- and regional-scale haze events, Environ. Sci. Technol., 48, 12002-  
1005 12011, doi: 10.1021/es503102w, 2014.

1006 Liu, X., Zhang, Y., Han, W., Tang, A., Shen, J., Cui, Z., Vitousek, P., Erisman, J. W.,  
1007 Goulding, K., Christie, P., Fangmeier, A., and Zhang, F.: Enhanced nitrogen  
1008 deposition over China, Nature, 494, 459-463, doi: 10.1038/nature11917, 2013b.

1009 Lu, Z., Streets, D. G., de Foy, B., Lamsal, L. N., Duncan, B. N., and Xing, J.: Emissions  
1010 of nitrogen oxides from US urban areas: estimation from Ozone Monitoring  
1011 Instrument retrievals for 2005-2014, Atmos. Chem. Phys., 15, 10367-10383, doi:  
1012 10.5194/acp-15-10367-2015, 2015.

1013 Michalski, G., Scott, Z., Kabling, M., and Thiemens, M. H.: First measurements and  
1014 modeling of  $\Delta^{17}\text{O}$  in atmospheric nitrate, Geophys. Res. Lett., 30, 1870-1872, doi:  
1015 10.1029/2003gl017015, 2003.

1016 Miyazaki, K., Eskes, H., Sudo, K., Boersma, K. F., Bowman, K., and Kanaya, Y.:  
1017 Decadal changes in global surface NO<sub>x</sub> emissions from multi-constituent satellite  
1018 data assimilation, Atmos. Chem. Phys., 17, 807-837, doi: 10.5194/acp-17-807-2017,  
1019 2017.

1020 Morin, S., Savarino, J., Frey, M. M., Yan, N., Bekki, S., Bottenheim, J. W., and Martins,  
1021 J. M.: Tracing the origin and fate of NO<sub>x</sub> in the Arctic atmosphere using stable  
1022 isotopes in nitrate, Science, 322, 730-732, doi: 10.1126/science.1161910, 2008.

1023 Morino, Y., Kondo, Y., Takegawa, N., Miyazaki, Y., Kita, K., Komazaki, Y., Fukuda,  
1024 M., Miyakawa, T., Moteki, N., and Worsnop, D. R.: Partitioning of HNO<sub>3</sub> and  
1025 particulate nitrate over Tokyo: Effect of vertical mixing, J. Geophys. Res., 111, doi:  
1026 10.1029/2005JD006887, 2006.

1027 Park, Y. M., Park, K. S., Kim, H., Yu, S. M., Noh, S., Kim, M. S., Kim, J. Y., Ahn, J. Y.,  
1028 Lee, M. D., Seok, K. S., and Kim, Y. H.: Characterizing isotopic compositions of TC-  
1029 C, NO<sub>3</sub><sup>-</sup>-N, and NH<sub>4</sub><sup>+</sup>-N in PM<sub>2.5</sub> in South Korea: Impact of China's winter heating,  
1030 Environ. Pollut., 233, 735-744, doi: 10.1016/j.envpol.2017.10.072, 2018.

1031 [Parnell, A. C., Phillips, D. L., Bearhop, S., Semmens, B. X., Ward, E. J., Moore, J. W.,](#)  
1032 [Jackson, A. L., Grey, J., Kelly, D. J., and Inger, R.: Bayesian stable isotope mixing](#)  
1033 [models. Environmetrics, 24, 387-399, doi: 10.1002/env.2221, 2013.](#)

1034 [Phillips, D. L., Inger, R., Bearhop, S., Jackson, A. L., Moore, J. W., Parnell, A. C.,](#)

- 1035 [Semmens, B. X., and Ward, E. J.: Best practices for use of stable isotope mixing](#)  
1036 [models in food-web studies, \*Can. J. Zool.\*, 92, 823-835, doi: 10.1139/cjz-2014-0127,](#)  
1037 [2014.](#)
- 1038 Price, C., Penner, J., and Prather, M.: NO<sub>x</sub> from lightning: 1. Global distribution based  
1039 on lightning physics, *J. Geophys. Res.*, 102, 5929-5941, doi: 10.1029/96JD03504,  
1040 1997.
- 1041 Reuter, M., Buchwitz, M., Hilboll, A., Richter, A., Schneising, O., Hilker, M., Heymann,  
1042 J., Bovensmann, H., and Burrows, J. P.: Decreasing emissions of NO<sub>x</sub> relative to CO<sub>2</sub>  
1043 in East Asia inferred from satellite observations, *Nat. Geosci.*, 7, 792-795, doi:  
1044 10.1038/ngeo2257, 2014.
- 1045 Richter, A., Burrows, J. P., Nüß, H., Granier, C., and Niemeier, U.: Increase in  
1046 tropospheric nitrogen dioxide over China observed from space, *Nature*, 437, 129, doi:  
1047 10.1038/nature04092, 2005.
- 1048 Savarino, J., Kaiser, J., Morin, S., Sigman, D., and Thiemens, M.: Nitrogen and oxygen  
1049 isotopic constraints on the origin of atmospheric nitrate in coastal Antarctica, *Atmos.*  
1050 *Chem. Phys.*, 7, 1925-1945, doi: 10.5194/acp-7-1925-2007, 2007.
- 1051 Seinfeld, J. H., and Pandis, S. N.: Atmospheric chemistry and physics: From air  
1052 pollution to climate change, John Wiley & Sons, 2012.
- 1053 [Shiraiwa, M., Pöschl, U., and Knopf, D. A.: Multiphase chemical kinetics of NO<sub>3</sub>](#)  
1054 [radicals reacting with organic aerosol components from biomass burning, \*Environ.\*](#)  
1055 [\*Sci. Technol.\*, 46, 6630-6636, doi: 10.1021/es300677a, 2012.](#)
- 1056 Sigman, D. M., Casciotti, K. L., Andreani, M., Barford, C., Galanter, M., and Böhlke,  
1057 J. K.: A bacterial method for the nitrogen isotopic analysis of nitrate in seawater and  
1058 freshwater, *Anal. Chem.*, 73, 4145-4153, doi: 10.1021/ac010088e, 2001.
- 1059 Simoneit, B. R. T., Schauer, J. J., Nolte, C. G., Oros, D. R., Elias, V. O., Fraser, M. P.,  
1060 Rogge, W. F., and Cass, G. R.: Levoglucosan, a tracer for cellulose in biomass  
1061 burning and atmospheric particles, *Atmos. Environ.*, 33, 173-182, *Anal. Chem.*, doi:  
1062 10.1016/S1352-2310(98)00145-9, 1999.
- 1063 Simoneit, B. R. T.: Biomass burning - a review of organic tracers for smoke from  
1064 incomplete combustion, *Appl. Geochem.*, 17, 129-162, *Anal. Chem.*, doi:  
1065 10.1016/S0883-2927(01)00061-0, 2002.
- 1066 Smith, M. L., Bertram, A. K., and Martin, S. T.: Deliquescence, efflorescence, and  
1067 phase miscibility of mixed particles of ammonium sulfate and isoprene-derived  
1068 secondary organic material, *Atmos. Chem. Phys.*, 12, 9613-9628, doi: 10.5194/acp-  
1069 12-9613-2012, 2012.
- 1070 Solomon, S., Qin, D., Manning, M., Chen, Z., Marquis, M., Averyt, K. B., Tignor, M.,  
1071 and Miller, H. L.: Climate change 2007: The physical science basis: contribution of  
1072 Working Group I to the Fourth Assessment Report of the Intergovernmental Panel on  
1073 Climate Change, Cambridge University Press, New York, 2007.
- 1074 Thiemens, M. H., and Heidenreich, J. E.: The mass-independent fractionation of oxygen:  
1075 a novel isotope effect and its possible cosmochemical implications, *Science*, 219,  
1076 1073-1075, doi: 10.1126/science.219.4588.1073, 1983.
- 1077 Thiemens, M. H.: Mass-independent isotope effects in planetary atmospheres and the  
1078 early solar system, *Science*, 283, 341-345, doi: 10.1126/science.283.5400.341, 1999.

带格式的: 正文, 左, 缩进: 左侧: 0 厘米, 悬挂缩进: 1 字符,  
首行缩进: -1 字符

1079 Turekian, V. C., Macko, S., Ballentine, D., Swap, R. J., and Garstang, M.: Causes of  
1080 bulk carbon and nitrogen isotope fractionations in the products of vegetation burns:  
1081 laboratory studies, *Chem. Geol.*, 152, 181-192, doi: 10.1016/S0009-2541(98)00105-  
1082 3, 1998.

1083 Walters, W. W., Goodwin, S. R., and Michalski, G.: Nitrogen stable isotope composition  
1084 ( $\delta^{15}\text{N}$ ) of vehicle-emitted  $\text{NO}_x$ , *Environ. Sci. Technol.*, 49, 2278-2285, doi:  
1085 10.1021/es505580v, 2015.

1086 Walters, W. W., and Michalski, G.: Theoretical calculation of nitrogen isotope  
1087 equilibrium exchange fractionation factors for various  $\text{NO}_y$  molecules, *Geochim.*  
1088 *Cosmochim. Ac.*, 164, 284-297, doi: 10.1016/j.gca.2015.05.029, 2015.

1089 Walters, W. W., and Michalski, G.: Theoretical calculation of oxygen equilibrium  
1090 isotope fractionation factors involving various  $\text{NO}_y$  molecules, OH, and  $\text{H}_2\text{O}$  and its  
1091 implications for isotope variations in atmospheric nitrate, *Geochim. Cosmochim. Ac.*,  
1092 191, 89-101, doi: 10.1016/j.gca.2016.06.039, 2016.

1093 Walters, W. W., Simonini, D. S., and Michalski, G.: Nitrogen isotope exchange between  
1094  $\text{NO}$  and  $\text{NO}_2$  and its implications for  $\delta^{15}\text{N}$  variations in tropospheric  $\text{NO}_x$  and  
1095 atmospheric nitrate, *Geophys. Res. Lett.*, 43, 440-448, doi: 10.1002/2015gl066438,  
1096 2016.

1097 Wang, H., Lu, K., Chen, X., Zhu, Q., Chen, Q., Guo, S., Jiang, M., Li, X., Shang, D.,  
1098 Tan, Z., Wu, Y., Wu, Z., Zou, Q., Zheng, Y., Zeng, L., Zhu, T., Hu, M., and Zhang,  
1099 Y.: High  $\text{N}_2\text{O}_5$  concentrations observed in urban Beijing: Implications of a large  
1100 nitrate formation pathway, *Environ. Sci. Technol. Lett.*, 4, 416-420, doi:  
1101 10.1021/acs.estlett.7b00341, 2017.

1102 Wankel, S. D., Chen, Y., Kendall, C., Post, A. F., and Paytan, A.: Sources of aerosol  
1103 nitrate to the Gulf of Aqaba: Evidence from  $\delta^{15}\text{N}$  and  $\delta^{18}\text{O}$  of nitrate and trace metal  
1104 chemistry, *Mar. Chem.*, 120, 90-99, doi: 10.1016/j.marchem.2009.01.013, 2010.

1105 Wojtal, P. K., Miller, D. J., O'Conner, M., Clark, S. C., and Hastings, M. G.: Automated,  
1106 high-resolution mobile collection system for the nitrogen isotopic analysis of  $\text{NO}_x$ , *J.*  
1107 *Vis. Exp.*, 118, e54962, doi: 10.3791/54962, 2016.

1108 Yienger, J. J., and Levy, H.: Empirical model of global soil-biogenic  $\text{NO}_x$  emissions, *J.*  
1109 *Geophys. Res.*, 100, 11447-11464, doi: 10.1029/95JD00370, 1995.

1110 Zhang, Q., Geng, G., Wang, S., Richter, A., and He, K.: Satellite remote sensing of  
1111 changes in  $\text{NO}_x$  emissions over China during 1996-2010, *Chinese Sci. Bull.*, 57,  
1112 2857-2864, doi: 10.1007/s11434-012-5015-4, 2012.

1113 Zhang, R., Tie, X., and Bond, D. W.: Impacts of anthropogenic and natural  $\text{NO}_x$  sources  
1114 over the U.S. on tropospheric chemistry, *P. Natl. Acad. Sci. U.S.A.*, 100, 1505-1509,  
1115 doi: 10.1073/pnas.252763799, 2003.

1116 Zhao, B., Wang, S. X., Liu, H., Xu, J. Y., Fu, K., Klimont, Z., Hao, J. M., He, K. B.,  
1117 Cofala, J., and Amann, M.:  $\text{NO}_x$  emissions in China: historical trends and future  
1118 perspectives, *Atmos. Chem. Phys.*, 13, 9869-9897, doi: 10.5194/acp-13-9869-2013,  
1119 2013.

1120 Zhao, Y., Qiu, L. P., Xu, R. Y., Xie, F. J., Zhang, Q., Yu, Y. Y., Nielsen, C. P., Qin, H.  
1121 X., Wang, H. K., Wu, X. C., Li, W. Q., and Zhang, J.: Advantages of a city-scale  
1122 emission inventory for urban air quality research and policy: the case of Nanjing, a

1123 typical industrial city in the Yangtze River Delta, China, *Atmos. Chem. Phys.*, 15,  
1124 12623-12644, doi: 10.5194/acp-15-12623-2015, 2015.  
1125 Zong, Z., Wang, X., Tian, C., Chen, Y., Fang, Y., Zhang, F., Li, C., Sun, J., Li, J., and  
1126 Zhang, G.: First assessment of NO<sub>x</sub> sources at a regional background site in North  
1127 China using isotopic analysis linked with modeling, *Environ. Sci. Technol.*, 51, 5923-  
1128 5931, doi: 10.1021/acs.est.6b06316, 2017.

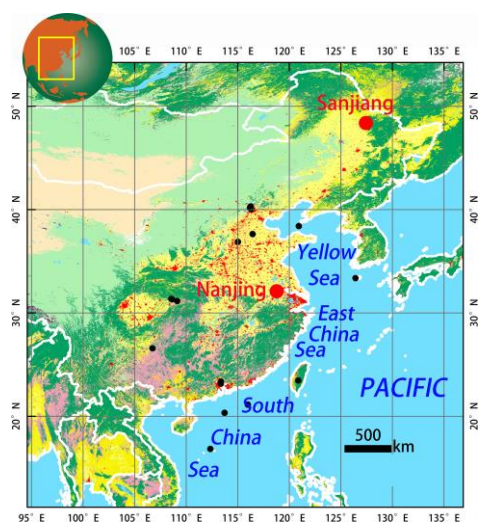
1129  
1130

1131

1132

1133

1134



1135

1136 **Figure 1.** Location of the sampling sites Sanjiang and Nanjing. The black dots  
1137 indicate the location of sampling sites (sites are located in the area of mainland China  
1138 and the Yellow and East and South China Seas) with  $\delta^{15}\text{N}\text{-NO}_3^-$  data from the  
1139 literature (see also Table S4).

1140

1141  
1142  
1143  
1144  
1145  
1146  
1147  
1148  
1149  
1150  
1151  
1152  
1153  
1154  
1155  
1156  
1157  
1158  
1159

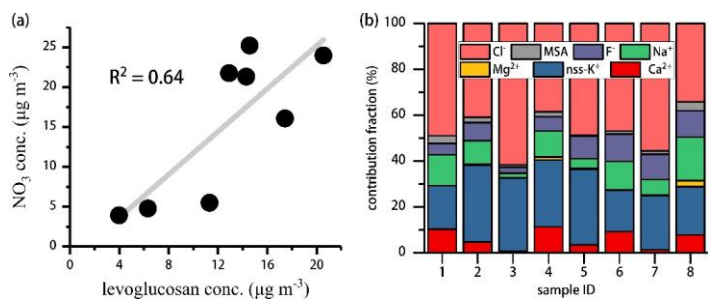


**Figure 2.** (a) Correlation analysis between the mass concentrations of levoglucosan and aerosol nitrate during the Sanjiang sampling campaign; (b) Variation of fractions of various inorganic species (MSA stands for methyl sulphonate) during day-night samplings at Sanjiang between 8 and October 2013 18 (sample ID 1 to 8, respectively). The higher relative abundances of  $\text{nss-K}^+$  and  $\text{Cl}^-$  are indicative for a biomass-burning dominated source. For sample ID information and exact sampling dates, refer to Table S3.

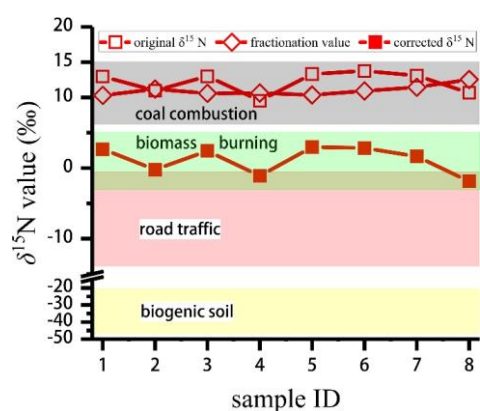
带格式的: 上标



1160

1161

1162



1163

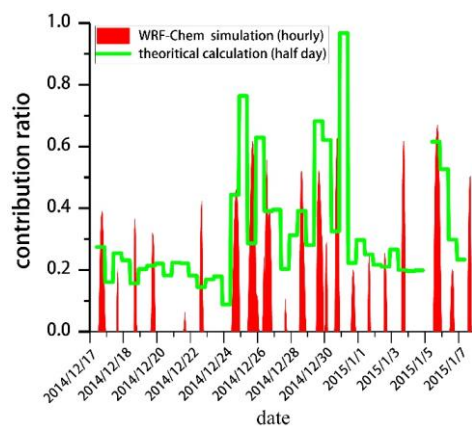
1164 **Figure 3.** Original  $\delta^{15}\text{N}$  values ( $\delta^{15}\text{N}_{\text{ini}}$ ) for  $p\text{NO}_3^-$ , calculated values for the N isotope  
1165 fractionation ( $\epsilon_{\text{N}}$ ) associated with the conversion of gaseous  $\text{NO}_x$  to  $p\text{NO}_3^-$ , and  
1166 corrected  $\delta^{15}\text{N}$  values ( $\delta^{15}\text{N}_{\text{corr}}$ ;  $^{15}\text{N}_{\text{ini}}$  minus  $\epsilon_{\text{N}}$ ) of  $p\text{NO}_3^-$  for each sample collected  
1167 during the Sanjiang sampling campaign. The colored bands represent the variation  
1168 range of  $\delta^{15}\text{N}$  values for different  $\text{NO}_x$  sources based on reports from the literature  
1169 (Table S2). See Table S3 for the information regarding sample ID.

1170

1171

1172

1173



1174

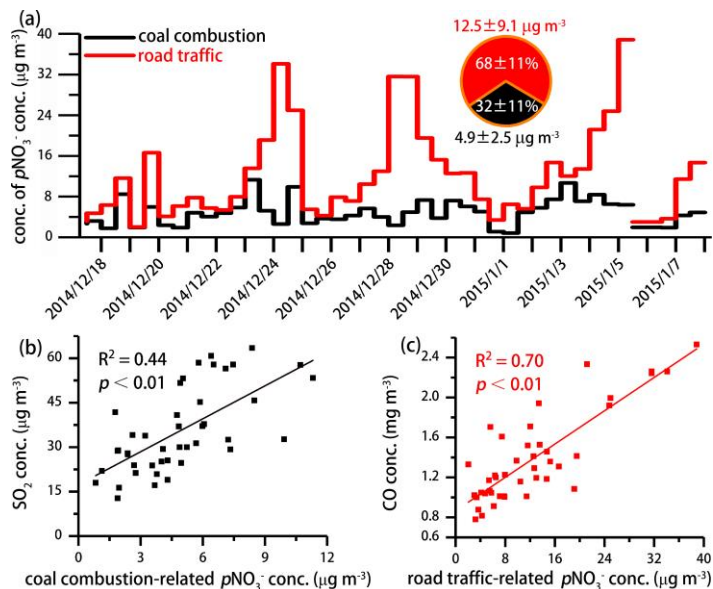
1175 **Figure 4.** Comparison between the theoretical calculation and WRF-Chem simulation  
 1176 of the average contribution ratio ( $\gamma$ ) for nitrate formation in Nanjing via the reaction  
 1177 of  $\text{NO}_2$  and photochemically produced  $\bullet\text{OH}$ .

1178

1179

1180

1181



1182

1183 **Figure 5.** (a) Time-series variation of coal combustion and road traffic contribution to  
 1184 the mass concentrations of ambient  $p\text{NO}_3^-$  in Nanjing, as estimated through MixSIR;  
 1185 (b) Correlation analysis between the mass concentrations of coal combustion-related  
 1186  $p\text{NO}_3^-$  and  $\text{SO}_2$ ; (c) Correlation analysis between the mass concentrations of road  
 1187 traffic-related  $p\text{NO}_3^-$  and CO.

1188

1189

1190

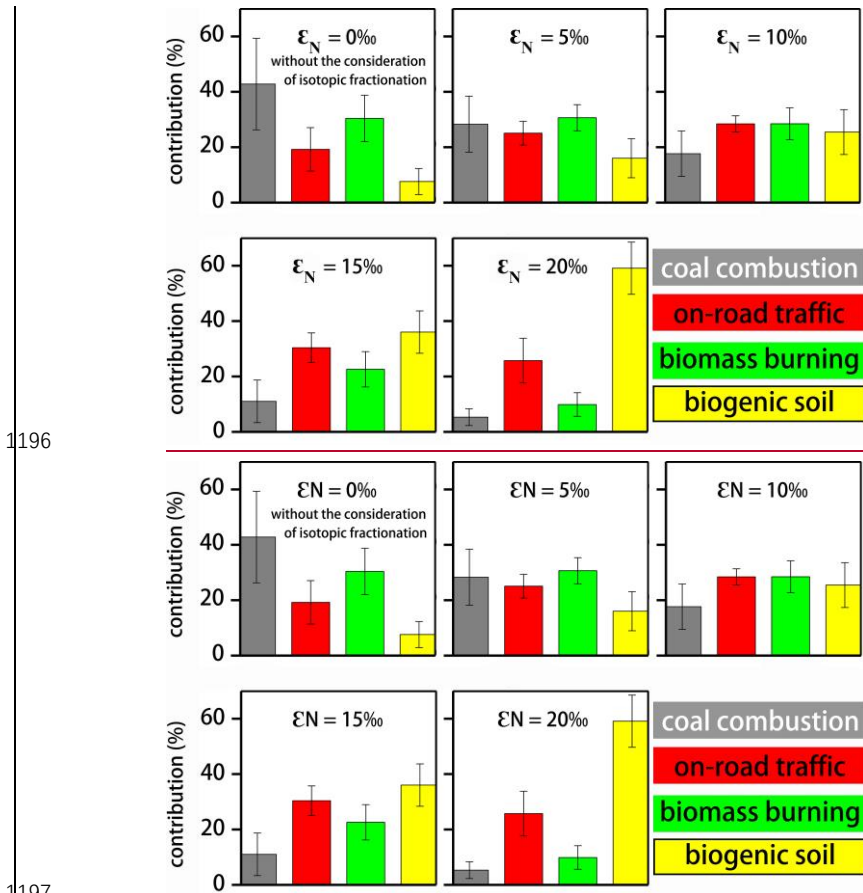
1191

1192

1193

1194

1195



1196

1197

1198

1199

1200

1201

**Figure 6.** Estimates of the relative importance of single  $\text{NO}_x$  sources (mean  $\pm 1\sigma$ ) throughout China based on the original  $\delta^{15}\text{N-NO}_3^-$  values extracted from the literature ( $\epsilon_N = 0\text{‰}$ ) and under consideration of significant N isotope fractionation during  $\text{NO}_x$  transformation ( $\epsilon_N = 5\text{‰}$ ,  $10\text{‰}$ ,  $15\text{‰}$  or  $20\text{‰}$ ).